

석사학위논문

일차원 U-Net 기반의 비침습 연속 혈압 파형 추정

**Non-invasive Continuous Arterial Blood  
Pressure Waveform Estimation Using 1-D U-  
Net**

국민대학교 일반대학원

전자공학과 전자공학전공

**Tasbiraha Athaya**

**2020**

**Non-invasive Continuous Arterial Blood Pressure Waveform  
Estimation Using 1-D U-Net**

*by*  
*Tasbiraha Athaya*

A thesis Submitted to the Department of Electronics Engineering, Graduate School, Kookmin University in partial fulfillment of the requirements for the degree of Master of Science

*Supervised by*  
**Professor Sunwoong Choi**

2020 년 4 월

**Graduate School, Kookmin University  
Department of Electronics Engineering  
2020**

# **Non-invasive Continuous Arterial Blood Pressure Waveform Estimation Using 1-D U-Net**

A thesis Submitted in partial fulfillment of the requirements for the degree of Master of  
Science

*by*

*Tasbiraha Athaya*

July 2021

This is certified that it is fully adequate in scope and quality as a thesis for the degree of  
Master of Science

Approved by

---

Professor Ki-Doo Kim (Chair, Thesis committee)

---

Professor Sunwoong Choi (Thesis supervisor & member, Thesis committee)

---

Professor Soochahn Lee (Member, Thesis committee)

**Graduate School, Kookmin University  
Department of Electronics Engineering  
2020**

Tasbiraha Athaya 의

석사학위 청구논문을 인준함

2021년 7월

심사위원장 김기두 

심사위원 최선웅 

심사위원 이수찬 

국민대학교 일반대학원

*Dedicated  
to  
My Family*

## **Acknowledgment**

First and foremost, I am very grateful and thankful to Almighty God, the most amiable, for giving me the opportunity to complete my Master's study. At the same time, would like to express my sincere gratefulness to my supervisor, Prof. Sunwoong Choi, for his scholastic guidance, continuous support, and inspiration throughout my entire Master's study. Without his active support, I may not have found myself at Master's study. I am really obliged to gain his trust in me and his insightful advice has been beneficial for me. I would like to express my gratitude to my all course teachers from whom I learn many recent outstanding theories and technological knowledge. My deep heartiest gratitude is for the thesis committee members who have invested their time and valuable knowledge for improving this thesis in an auspicious manner. I would like to express my deep-hearted respect and gratefulness to Prof. Ki-Doo Kim and Prof. Soochahn Lee for their deep supervision and assessment of my dissertation. After that, Kookmin University also deserves this acknowledgment. I am indebted to Kookmin University authority for providing me sufficient facilities and opportunities throughout my entire Master's study. I am also thankful to the Korean Government for giving me the precious opportunity to study here in the Republic of Korea.

It is a great honor and always prestigious for me to be a member of the Network Computing Lab. Thanks to my dearest lab mates, who are always enlightening my inspiration to direct me into my goal. I want to provide my confession to all of my Bangladeshi friends, juniors, and senior brothers living in Korea, for their boundless care and support during my stay in Korea.

And last but not the least; I am indebted to my dearest parents, S.M. Bazlur Rashid and Sultana Rabeya. And my dear husband, M Shifat Hossain, for making me focused on my goals, and also for their continuous support, enormous inspiration, and contribution in every aspect of my life.

## Table of Contents

Acknowledgment .....	i
Table of Contents .....	ii
List of Figures .....	v
List of Tables .....	vi
Abstract .....	vii
Introduction .....	1
1.1    Blood Pressure .....	1
1.1.1    Blood Pressure and Human Health .....	1
1.1.2    ABP Waveform .....	2
1.1.3    BP Ranges .....	3
1.2    BP Measurement Techniques .....	3
1.2.1    Invasive Technique .....	3
1.2.2    Non-invasive Technique .....	3
1.3    Problems in Conventional BP Measurement .....	4
1.3.1    Problems of Invasive Method .....	4
1.3.2    Problems of Cuff-based Non-invasive Method .....	4
1.4    Proposed Solution .....	5
1.5    Photoplethysmogram .....	6
1.5.1    Principle of PPG .....	6
1.5.2    PPG Waveform .....	6
1.5.3    Usage of PPG .....	7
1.5.4    Android Applications .....	7
1.5.5    Other PPG Based Systems .....	8
Related Works .....	9
2.1    Correlation Between PPG and ABP .....	9

2.2	ABP Waveform Estimation Approaches .....	10
2.3	Bio-signals for BP Measurement.....	10
2.3.1	Photoplethysmogram (PPG) and Electrocardiogram (ECG) .....	10
2.3.2	Photoplethysmogram (PPG) and Seismocardiogram (SCG) .....	10
2.3.3	Photoplethysmogram (PPG) and Ballistocardiogram (BCG) .....	11
2.3.4	PPG Signal Only .....	11
2.4	BP Measurement Devices.....	12
	Methodology .....	13
3.1	Data Collection.....	13
3.1.1	MIMIC Database .....	14
3.1.2	MIMIC-III Waveform Database.....	14
3.2	Data Pre-processing.....	14
3.2.1	PPG Filtering .....	15
3.2.2	Windowing PPG and ABP.....	15
3.2.3	Phase Matching.....	16
3.2.4	Normalization .....	17
3.2.5	Pre-processed Final Dataset.....	17
3.3	U-net Architecture .....	18
3.3.1	Contracting Path.....	19
3.3.2	Expansion Path.....	19
3.4	Squeeze U-net Architecture.....	19
3.4.1	Contracting Path.....	21
3.4.2	Expansion Path.....	22
3.5	ABP Waveform Estimation Process.....	23
	Result Evaluation .....	24
4.1	Hyper-Parameter and Equipment Setup .....	24
4.2	Predicted Continuous and Non-Invasive ABP Waveform Analysis Results .....	25

4.3	SBP and DBP Estimation Results .....	26
4.4	Compliance with Standards.....	30
4.5	Comparison Between U-net and Squeeze U-net Models .....	31
4.6	Comparison with Related Works.....	33
	Application Development .....	37
5.1	BP Calculator.....	37
5.2	BP Measurement Process .....	37
5.3	Advantages of BP Calculator .....	38
5.4	Disadvantages of BP Calculator .....	39
	Discussion and Conclusion .....	40
6.1	Discussion.....	40
6.2	Future Research Opportunities .....	41
6.3	Conclusion.....	41
	References.....	42

## List of Figures

Figure 1. ABP waveform .....	2
Figure 2. Chart of four blood pressure ranges .....	3
Figure 3. An ideal single PPG waveform .....	7
Figure 4. Flow chart of the overall workflow .....	13
Figure 5. Windowing of PPG and ABP signals .....	15
Figure 6. Conventional PPG and ABP measurement method .....	16
Figure 7. Phase difference matching between PPG and ABP waveforms. (a) Measured Signals; (b) Delay estimation between signals after cross-correlation; (c) Shifting ABP by estimated delay .....	17
Figure 8. Distribution of SBP and DBP values .....	18
Figure 9. The architecture of the proposed U-net deep learning model .....	18
Figure 10. The architecture of Squeeze U-net deep learning model .....	20
Figure 11. The structure of a fire module of Squeeze U-net .....	21
Figure 12. Loss versus epochs curves for (a) U-net and (b) Squeeze U-net model .....	24
Figure 13. Predicted ABP waveform from PPG of a subject. (a) Input PPG signal; (b) Reference ABP signal and Predicted ABP signal .....	25
Figure 14. Distribution of Pearson's correlation coefficient .....	26
Figure 15. Error histograms of predicted SBP and DBP values using U-net .....	27
Figure 16. Error histograms of predicted SBP and DBP values using Squeeze U-net .....	27
Figure 17. Prediction accuracy of SBP and DBP values in four BP ranges using U-net .....	28
Figure 18. Prediction accuracy of SBP and DBP values in four BP ranges using Squeeze U-net .....	28
Figure 19. Linear regression plot of the SBP, DBP, and MAP result using U-net .....	29
Figure 20. Linear regression plot of the SBP, DBP, and MAP result using Squeeze U-net .....	29
Figure 21. Bland–Altman scatterplot for predicted SBP and DBP values using U-net .....	30
Figure 22. Bland–Altman scatterplot for predicted SBP and DBP values using Squeeze U-net .....	30
Figure 23. Blood pressure measurement process using “BP Calculator” application .....	38

## List of Tables

Table 1. Performance summary of U-net model on test dataset for ABP waveform prediction.	26
Table 2. Performance detail of U-net and Squeeze U-net models for SBP, DBP, and MAP values measurement.	26
Table 3. Comparison of our result with the Association for the Advancement of Medical Instrumentation (AAMI) standard.	31
Table 4. Comparison of the result with British Hypertension Society (BHS) grading standard.	31
Table 5. Comparison of the number of U-net and Squeeze U-net parameters in contraction path.	31
Table 6. Comparison of the number of U-net and Squeeze U-net parameters in Expansion path.	32
Table 7. Quantitate comparison between U-net and Squeeze U-net regarding model size, number of operations and prediction time.	33
Table 8. Result comparison with related works.	34
Table 9. Comparison with related works using our pre-processed PPG signal.	35
Table 10. Quantitate comparison among Squeeze U-net model with related works.	36

## Abstract

# Non-invasive Continuous Arterial Blood Pressure Waveform Estimation Using 1-D U-Net

By Tasbiraha Athaya

Department of Electronics Engineering

Graduate School, Kookmin University

Seoul, Korea

In this research, a non-invasive arterial blood pressure (ABP) waveform monitoring technique has been proposed. The ABP waveform is obtained from non-invasive fingertip photoplethysmogram (PPG) signal using as the input of deep learning modified U-net network. From the ABP waveform, systolic blood pressure (SBP), diastolic blood pressure (DBP), and mean arterial pressure (MAP) were measured. To build an android application named “BP Calculator” to measure SBP and DBP regularly, an energy efficient modified Squeeze U-net model is used. An evaluation of the proposed two methods is performed on a subset of 100 individuals from two publicly available databases. One is the MIMIC and another is the MIMIC-III waveform database. The ABP waveforms predicted from PPG using U-net model, are highly correlated with the reference ABP waveforms of the databases. An average Pearson’s correlation coefficient of 0.993 is obtained for the predicted ABP waveforms using U-net. The mean absolute error (MAE) is  $3.68 \pm 4.42$  mmHg and  $4.42 \pm 4.78$  mmHg for SBP,  $1.97 \pm 2.92$  mmHg and  $2.25 \pm 2.98$  mmHg for DBP, and  $2.17 \pm 3.06$  mmHg and  $2.56 \pm 3.21$  mmHg for MAP using U-net and Squeeze U-net models, respectively. The result of the Squeeze U-net model is slightly lower than the U-net model, but both of the models satisfy the requirements of the Association for the Advancement of Medical Instrumentation (AAMI) standard and obtain grade A according to the British Hypertension Society (BHS) standard.

**Keywords:** Arterial Blood Pressure, Photoplethysmogram, U-net, Squeeze U-net.

# Chapter 1

## Introduction

### 1.1 Blood Pressure

Blood pressure (BP) is the pressure in the aorta and its branches. It is the force of blood against the walls of our arteries. The arteries carry blood from our heart to other parts of our body. However, BP can become seriously high, and it can also get extremely low. Our BP is highest as it leaves our heart and enters the aorta, and it is lowest when it reaches the end of its journey through successively lower branches of arteries. Blood circulates around our body because of the difference in pressure.

#### 1.1.1 Blood Pressure and Human Health

Blood pressure generates a force which is important because nutrients as well as oxygen would not be pumped to the circulatory system without BP to nurture organs and tissues. BP is also important because it transports white blood cells and antibodies, as well as hormones like insulin, for immunity. Blood has a number of other characteristics, including maintaining the temperature. It also contains clotting platelets, which limit blood loss after an accident and are one of our protections against tissue damage. Blood pressure is affected by the state of the arteries. Narrowing of the arteries can lead to complete blockage of the supply, resulting in hazardous diseases such as heart attacks and strokes.

Blood pressure (BP) monitoring and management in the normal range is vital to a healthy life. Fluctuation in BP has a strong correlation with several organ injuries in the case of hypertension or high BP [1]. Hypertension is identified as one of the major risks for ischemic heart disease. According to the World Heart Federation, about 50 percent of ischemic strokes are caused by hypertension [2]. Furthermore, it also increases the risk of hemorrhagic stroke, heart failure, heart attack, and chronic kidney disease[2], [3]. The number of persons suffering from hypertension is expected to reach 1.5 billion by 2025. Any healthcare system would be overburdened by the consequences of this sickness. [4].

### 1.1.2 ABP Waveform

The arterial blood pressure waveform is usually acquired from the brachial artery. In ABP waveform, the highest peaks denote SBP and the valleys denote DBP. MAP is the average pressure in the arteries during a cardiac cycle as shown in Figure 2. SBP is the maximum pressure within the large arteries when the heart muscle contracts to flow blood through the body. And DBP refers to the lowest pressure within the large arteries during heart muscle relaxation between each beat [5].

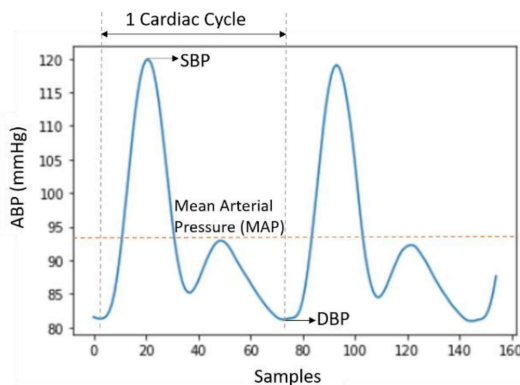


Figure 1. ABP waveform.

ABP waveform can provide additional information to the doctors more than just SBP and DBP values [6]. So, the regular measurement of SBP and DBP still cannot replace the use of monitoring invasive ABP waveform for critical care patients. ABP waveform can provide following advantages:

- The ABP waveform gives mean arterial pressure (MAP) which indicates perfusion pressure in the vital organs of the body better than SBP [7].
- The waveform also can identify the problems that lead to hypertension [8]. For example, the ABP waveform provides information about arterial stiffness which can be optimized for the treatment of high blood pressure [9].
- Moreover, the mathematical analysis of this waveform helps to estimate cardiac output [10] and stroke volume [11].
- ABP is used in ICUs and CCUs where extreme and rapid changes are expected in the blood pressure. For example, ABP waveform is monitored for the surgery patients of pheochromacytoma and certain dysrhythmias.

- The shape of ABP waveform provides useful information for the treatment of aortic valve disease.

### 1.1.3 BP Ranges

In [12], four blood pressure ranges of a person are given based on SBP and DBP. The four ranges are normal, pre-hypertension, stage-1 hypertension, and stage-2 hypertension as shown in Figure 3.

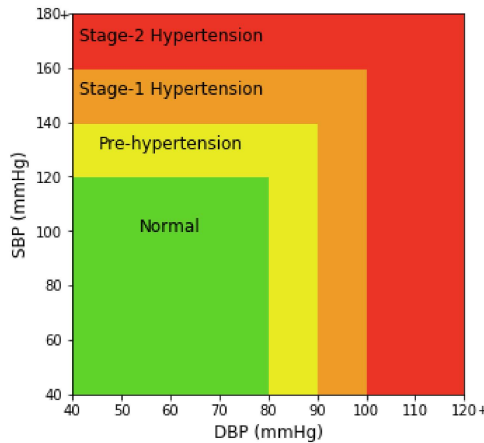


Figure 2. Chart of four blood pressure ranges.

## 1.2 BP Measurement Techniques

### 1.2.1 Invasive Technique

Invasive continuous BP measurement method is also known as direct BP measurement or invasive ABP. In this method, a catheter is inserted into an artery to conduct real-time BP monitoring. It can complete BP estimation in every cardiac cycle and monitor BP changes more precisely. Therefore, it is recognized internationally as the gold standard of BP monitoring methods [13]. This approach is used only for critical patients. The bloodstream is connected to a pressure transducer, which is commonly a column of incompressible fluid like saline, in order to monitor ABP waveform.

### 1.2.2 Non-invasive Technique

Traditionally and most commonly, the non-invasive auscultatory and oscillometric measurements is used to measure BP. The measurement result is expressed in terms of systolic BP (SBP) and diastolic BP (DBP). Recently, signal based continuous non-invasive blood

pressure measurement techniques are highly researched. The noninvasive measurement techniques are:

- **Auscultatory:** It needs a sphygmomanometer cuff along with a stethoscope to measure SBP and DBP. An inflated cuff attached to an aneroid or a mercury manometer is wrapped around at the upper arm at nearly the same vertical height as the heart.
- **Oscillometric:** As like as the auscultatory technique, the oscillometric technique uses a sphygmomanometer cuff to measure only SBP and DBP. But it uses these with an electronic pressure transducer to monitor oscillations of cuff pressure. The electronic transducer is used for automatically interpreting the result, and then automatically inflate and deflate the cuff. The pressure transducer need to be calibrated from time to time to maintain the accuracy.
- **Signal based methods:** Different bio-signals like photoplethysmogram (PPG), electrocardiogram (ECG), seismocardiogram (SCG), ballistocardiogram (BCG) etc. are being used to measure blood pressure in recent times. These signals can measure BP without using a cuff. But the results are not established yet and this field needs more research.

### 1.3 Problems in Conventional BP Measurement

#### 1.3.1 Problems of Invasive Method

- Requires arterial puncture
- High risk of complications and infection
- Painful for users.
- Kits are non-reusable.
- Monitoring equipment is needed to show the result.
- Regular re-initializing and re-levelling is required.
- Measurement needs to be done by trained professionals.
- Transducers have a tendency to drift.
- Equipment are relatively costly.

#### 1.3.2 Problems of Cuff-based Non-invasive Method

- The BP cuff should be always placed against bare skin. Because measurements that are taken from skin covered with clothes are usually less appropriate.

- The cuff size need to be of accurate size for the measurement sight. Cuffs that are undersized record too high BP and cuffs that are oversized may record too low BP.
- At extreme pressure, measurements can be less reliable.
- Monitoring BP continuously is not possible. So, many hypotensive cycles may be missed, that need more accurate and frequent detection.
- Can cause pain if frequent measurement is needed
- In case of patients with unstable BP, maximum accuracy needs manual process.

## 1.4 Proposed Solution

After discussing the problem in BP measurement, we wanted to give a solution for easy and comfortable measurement of BP. In order to give a solution, we conducted a research to build a BP measurement system using easily obtainable photoplethysmogram (PPG) signal with the help of deep learning model. Using PPG and deep learning algorithm both the problem associated with invasive measurement and cuff-based measurement can be solved. But to obtain a reliable and accurate result huge research is needed. So, our purpose is to provide a deep learning method for noninvasive continuous arterial blood pressure waveform measurement using PPG signal. From the waveform, widely used and most important SBP, DBP, and MAP values can be obtained.

Our contributions to this sector are given below:

- Estimating continuous and non-invasive ABP waveform directly from the PPG signal is new and efficient.
- Our proposed method provides SBP, DBP, and MAP values with improved accuracy.
- Our method does not need beat-segmentation of PPG signals
- Non-invasive, continuous, and rapid approach.
- Only PPG signal is required and there is no need to calculate features to estimate BP.
- The proposed models can be trained using a small dataset since they are simple and computationally very efficient.
- The method can be easily applied in a wearable sensor-based device or smartphone.

I would like to mention that a part of this work has been already presented and published in an international conference [14] and in Sensors journal [15].

To understand our BP measurement method, first of all it is important to know what is the PPG signal which will be the main input of our proposed deep learning model. So, the next section will discuss about this PPG signal and its applications.

## 1.5 Photoplethysmogram

Photoplethysmogram (PPG) is an optically obtained signal to detect blood volume changes at peripheral limbs. It is a non-invasive and cost efficient technique that can make measurements from the surface of our skin.

Photoelectric plethysmogram, also called photoplethysmogram, and its abbreviation in some cases is (PTG/PPG), and when it is referred to as digital volume pulse, the abbreviation is (DVP). The acronym PPG will be used throughout this writing.

### 1.5.1 Principle of PPG

Light waves in the visible, near UV, and infrared ranges are generally used to acquire PPG signals. Light waves pass through skin, fat, muscle, and bone tissues. These waves are absorbed and dispersed during transmission. Because blood samples absorb and scatter light waves considerably more than other tissues in the peripheral limbs, changes in blood volume may be determined by the light receiving using the photodetector.

This method contains information about the cardiovascular system and bodily compositions. Recent advances in this regard are trying to widely adopt this technology for non-invasive measurements of properties.

### 1.5.2 PPG Waveform

As stated previously, the PPG signal is a representation of the changes in the volume of blood at the measurement site. As this is a pulsatile waveform, it has two components – AC and DC. The DC component indicates respiratory changes and skin baseline absorption. The DC component is usually lower frequency PPG signals (not accurate 0Hz portion). On the other hand, the AC part indicates the change of blood volume in an artery. This indicates the cardiac cycle and corresponds to blood pressure.

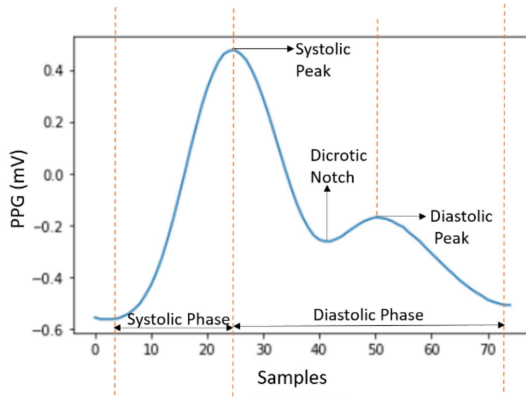


Figure 3. An ideal single PPG waveform.

A single PPG waveform with its properties is shown in Figure 1. A single waveform is consisted of a systolic peak, a diastolic peak and a dicrotic notch. From the starting of a waveform to the systolic peak is called systolic phase and from the systolic peak to the end of the waveform is diastolic phase.

### 1.5.3 Usage of PPG

In the clinical space, the PPG signal is utilized in the following applications:

- Blood oxygen saturation
- Heart rate
- Clinical physiological monitoring
- Blood pressure
- Respiration
- Cardiac output
- Arterial disease
- Other cardiovascular monitoring etc.

### 1.5.4 Android Applications

For chronic illness prevention and control, digital health techniques, particularly mobile health diagnostics, which is also known as mHealth diagnostics, have been proven to be effective, accessible, and long-term. Mobile phones are a widely used and easily accessible mHealth instrument. By utilizing the optical and computational power of smartphone, it could allow monitoring of biological information using the principle of informative PPG waveform [4].

The PPG sensor monitors fluctuations in intensity of light via transmission through or reflection from the skin cell using a smartphone application. Variations in light intensity are associated to changes in skin cell blood perfusion, and information about the heart can be derived based on these variations. [16], [17].

### **1.5.5 Other PPG Based Systems**

Many wearable devices have been developed based on PPG technologies. The most important property of a wearable device is to have a lower weight, power storage system, smaller in size and wearable functionalities, etc. Among all the applications, remote monitoring and telemedicine are the most promising applications that PPG systems can provide. If enough data can be estimated from PPG systems, this has a promising aspect in the future with telemedicine applications.

## Chapter 2

# Related Works

Epidemiological studies reveal that in developed countries, hypertension prevalence and control have reached a plateau since the middle of 2000s. Whereas, prevalence has surged in developing nations with poor states of consciousness and control. [18], [19]. Earlier detection and control of hypertension problems are crucial, but they rely on precise and accessible measurements. [4]. So, appropriate control of BP is the basis of both primary and secondary ischemic heart disease prevention [20]. With the advancement of technology, researches are done widely to measure BP more accurately within low cost. Almost every people has a smartphone in his/her hand. Wearable devices are becoming more and more popular. So, signals acquired using different sensors for accurate BP measurement is a widely research topic of recent times. In this chapter, some of the recent researches on BP measurement approaches using different signals will be discussed.

### 2.1 Correlation Between PPG and ABP

The motivation of this work is that a high similarity is observed between the PPG and ABP signals. In [21], the similarities in both of frequency and time domains between the two signals were analyzed. Pearson's correlation coefficient between the two signals was higher than 0.9 on average. In [22], the authors mainly focused on analyzing the feature-based similarity between ABP and PPG signals. The authors considered the features like average peak position, slope, time period, amplitude, and elasticity of the two signals. In the research, the peak value of both ABP and PPG signals was observed to occur in a constant time interval. The upstroke time period of both signals was found to have a little difference between 0.02 s to 0.1 s. But the period of heart cycle timing remained the same. Pearson's correlation coefficient for the elasticity with a peak to peak amplitude of ABP was 0.822. In [23], 15 cardiac surgery subjects were examined to categorize their BP on the basis of the shape of the PPG signal. The method presented good accuracy 98.4% and 97.8% for detecting episodes of low BP and high BP, respectively.

## 2.2 ABP Waveform Estimation Approaches

Due to the importance of ABP waveform, some ABP waveform measurement methods have been proposed including the vascular unloading technique and the tonometry method. In the vascular unloading technique, which is also called the volume clamped method, a cuff is placed over a finger to measure blood volume change using a light source and detector by increasing and decreasing cuff pressure in an interlocking control loop [24]. But using continuous pressure for a long time is harmful and uncomfortable. The tonometry method [25] uses a sensor to measure palpation on the radial artery and measure continuous, non-invasive ABP. But tonometry method needs precise positioning and it is extremely sensitive to movement relative to the accessed artery [26]. It is not a popular approach at present due to its artifacts and users' discomfort [27].

## 2.3 Bio-signals for BP Measurement

### 2.3.1 Photoplethysmogram (PPG) and Electrocardiogram (ECG)

Pulse transit time (PTT) based BP estimation methods are very popular research topic for signal based BP measurement. Most of the PTT-based methods focus on the combination of two signals, photoplethysmogram (PPG) and electrocardiogram (ECG). PTT is the time taken by a blood pulse to propagate from the heart to a peripheral site and it is inversely related to BP. In [28], an ECG and PPG signal feature-based BP estimation process was discussed. The feature set used in the study also included the PTT, that is the time difference between the R wave of ECG and systolic point of PPG. However, much research has stated that the R wave of ECG is not reliable to measure the beginning of a pulse, and the measuring equipment for ECG data acquisition is very complex and expensive, the sensors are also hard to find.

### 2.3.2 Photoplethysmogram (PPG) and Seismocardiogram (SCG)

In [29], a combination of PPG and SCG was applied in a wristwatch for SBP and DBP calculation. The device needed a high-resolution three-axis accelerometer sensor pressed to the sternum to measure heart vibrations. It is really difficult to develop and implement a very accurate accelerometer sensor and to take the measurement in a wired wearable-device setup. The authors used the Moens–Kortweg equation to calculate PTT from PPG and SCG with two subject-specific parameters. However, both of the parameters would differ for each subject

which makes the overall BP estimation process troublesome. Besides, two different sensors were used to capture PPG and SCG. So, calibration between the two signals for individual sensors was needed to match the time difference.

### **2.3.3 Photoplethysmogram (PPG) and Ballistocardiogram (BCG)**

The research work in [30] proposed PTT based subject specific BP estimation based on PPG and ballistocardiogram (BCG). Like SCG and ECG, skin contact is not needed in BCG. In [31] the authors stated that the duration between predetermined J peak in BCG signal and predetermined PPG systolic peak interrelated with SBP and DBP. Yet, it is not ready to be implemented in a wearable form factor.

### **2.3.4 PPG Signal Only**

Reviewing the difficulties of using a combination of signals, and as PPG is the most convenient signal to be used in wearable devices, researchers are trying to measure BP using only the PPG signal [32], [33].

In [32], a total of 22 spectral and morphological features were extracted from PPG signals to characterize the signal to determine SBP and DBP output. They used an artificial neural network (ANN) with their filtered 58,795 single PPG cycles. The filtering process was not clear. They claimed to work with 72 subjects. But in the publicly available MIMIC database among 72 subjects, only 55 subjects have both PPG and ABP signals. In their individual result table, they showed the result of subjects 262, 415, 450 whose either PPG or ABP signal was missing. The signals of subjects 488, 481, 479, 478, and many were absent in the downloaded database, yet they showed their result in the individual table which was confusing. So, these discrepancies undermine the robustness of their conclusions.

The study [33] also used 8 features of pre-processed PPG signals as the input for different machine learning methods and the output was SBP and DBP. They used linear regression, artificial neural network, decision tree, bagging and random forest regression models for predicting SBP and DBP values only. With their small data, random forest performed well with 100 decision trees. But different feature selection problem also persists in these studies. The total amount of data was also very small and the result was also not satisfactory. They needed beat segmentation to detect single PPG cycles. But segmenting beat in noisy signals is very

difficult and no generalize way works for beat segmentation in noisy signals. So, the process may work for some particular segments, but not for all segments.

The work in [34] used preprocessed raw PPG signal windows with the first and second derivatives as the input of their modified ResNet-GRU-based network to predict SBP and DBP. However, this ResNet-GRU-based model is computationally expensive as the learning efficiency of gated recurrent unit (GRU) is low and converges slowly [35]. They used data from MIMIC III waveform database. Their method does not satisfy the Association for the Advancement of Medical Instrumentation (AAMI) standard error range. Their model needs to be trained for every subject individually to obtain proper SBP and DBP result in prediction phase. They said this process is easy for their GPU based setup, but cannot be used for real-time devices.

Similarly, another research work [36], used a convolutional neural network (CNN) model to get SBP and DBP output giving a similar pre-processed raw PPG signal window with the first and second derivatives as the input to the network. But their method does not satisfy the Association for the Advancement of Medical Instrumentation (AAMI) standard error range.

All of the above mentioned cuff-less PPG-based blood pressure measurement methods are only limited to the estimation of normally used SBP and DBP values. But none of the methods predicted the highly informative ABP waveform which is still used in critical care units of hospitals and medical centers.

## 2.4 BP Measurement Devices

In recent time, with the development of wearable technology and smartphones, PPG has become most commonly used technique for monitoring cardiovascular health and detecting diseases using wearable devices and smartphones. Measuring heart rate, body temperature, oxygen saturation and physical activity is common. Recently, some devices have tried to estimate BP. Like Redha et al. [37] used wristband with PPG sensor, Holz et al. [38] showed the used of finger probe and eye-glass with PPG sensor, Zhang et al. [52] made use of armband with ECG and PPG sensors, Plante et al. [39] applied smartphone camera and microphone to capture PPG and heart sound to measure blood pressure. But these techniques need to be more developed for accurate estimation. However, most popular wearable device to measure blood pressure is OMRON watch. But it uses the conventional pressure based method [40].

## Chapter 3

### Methodology

The overall workflow of our continuous and non-invasive ABP waveform estimation method is shown using a flow chart in Figure 4. The process of estimating the ABP waveform using U-net is similar to our work of [15]. First, the data were collected from the two databases. Then pre-processing was performed on the obtained data to remove artifacts from the signals. After that, the proposed modified U-net model was trained, validated, and tested with the pre-processed data. Finally, the ABP waveform was obtained from the PPG waveform using the trained U-net and squeeze U-net model. Squeeze U-net model is used to build an android application to predict SBP and DBP values regularly at home.

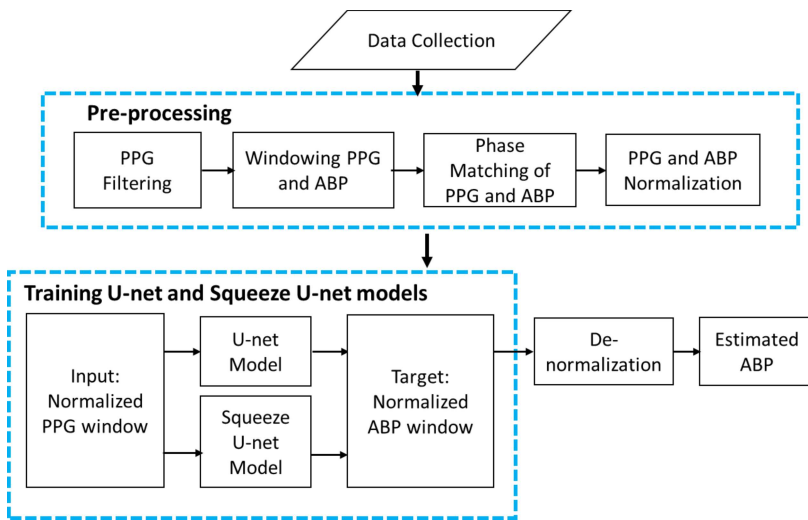


Figure 4. Flow chart of the overall workflow.

#### 3.1 Data Collection

The first block of Figure 4 shows the data collection step. The invasive ABP and fingertip PPG signals are used for the purpose of our research. The signals are obtained from a combination of two publicly available databases that contain data related to health. The databases contain simultaneous recordings of PPG (fingertip plethysmograph), ABP (arterial blood pressure), one or more ECG (Electrocardiogram), PAP (pulmonary arterial pressure), and CVP (central venous pressure). The names of the databases are given below:

- MIMIC (Multi-parameter Intelligent Monitoring in Intensive Care) database [41].
- MIMIC-III (Medical Information Mart for Intensive Care III) waveform database[42], [43].

### 3.1.1 MIMIC Database

MIMIC is a publicly available database that contains a myriad of recordings of 121 intensive care unit (ICU) patients. Each recording typically contains between 24 and 48 hours of continuous data recorded from patient monitors in the medical, surgical, and cardiac intensive care units of Boston's Beth Israel Hospital.

The recordings of every patient from bedside monitor is separated into hundreds of files. The files contain 10 minutes of recorded data. The files are assembled without any gaps to constitute continuous recordings. So, each recording is stored in an individual directory and given the name of the containing record. We downloaded these data from PhysioBank database which contains complete data of 72 patients.

In this study, we used recordings of 45 subjects consisting of both ABP and fingertip PPG signals with a 125 Hz sampling rate.

### 3.1.2 MIMIC-III Waveform Database

Another one is the MIMIC-III waveform database, which contains 67,830 records of approximately thirty thousand ICU patients. The signals are recorded from the bedside monitor in automated manner. Usually, the data files with a gap of at least 1 hour are split into separate records so that each record contain data from one subject.

A subset of 55 subjects of the MIMIC-III waveform database containing both PPG and ABP signals were selected for our experiment. Ultimately, 100 subjects' recordings were collected for the experiment, each with complete ABP and PPG signals.

## 3.2 Data Pre-processing

The second block of Figure 4 demonstrates the data pre-processing step. Data pre-processing was the most important and time-consuming part of this study.

### 3.2.1 PPG Filtering

First, PPG data were filtered using the Equiripple FIR filter with cutoff frequencies of 0.5 Hz to 8 Hz [37]. Values below 0.5 Hz were identified as baseline wandering, while values above 8 Hz were considered high-frequency noise. The FIR filter was selected as it is always stable with a linear phase. As we required the exact shape of the PPG signal, maintaining a constant phase was necessary. The filtering coefficients were calculated using the Matlab Filter Design and Analysis Tool. In the magnitude (dB) and phase response curve of the filter, the lower corner of the band-pass filter stop frequency was set to 0.1 Hz, the pass frequency was set to 0.5 Hz, and the stop attenuation was set to  $-60$  dB. For the higher corner, the pass frequency was set to 8 Hz, the stop frequency was set to 9 Hz, and the stop attenuation was set to  $-80$  dB. The PPG signals were filtered using 618 filtering coefficients.

### 3.2.2 Windowing PPG and ABP

After PPG signal filtering, the PPG and ABP signals were divided into windows of 350 samples sequentially with overlapping of 100 samples in Figure 5. The window size and overlap value were selected empirically, and overlapping was performed to avoid missing information at the boundary of the windows. Windows containing artifacts, that are inaccurate for measurement, were identified and removed using a machine learning model for signal artifact detection [14].

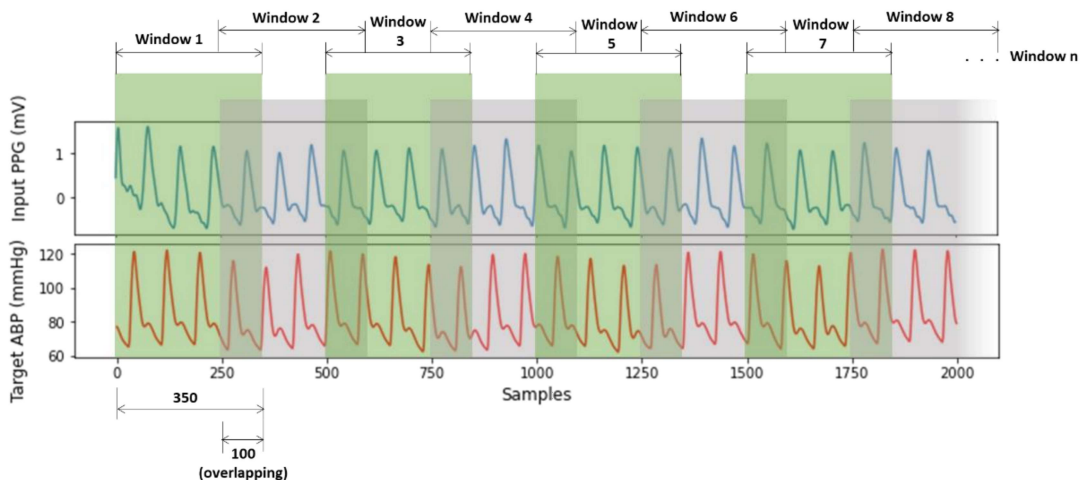


Figure 5. Windowing of PPG and ABP signals.

### 3.2.3 Phase Matching

After that, the ABP and PPG signals were phase-matched according to their phase difference. When blood flows from the brachial artery to the digital artery, ABP is measured from the brachial artery and PPG from the digital artery [44] as shown in Figure 6.

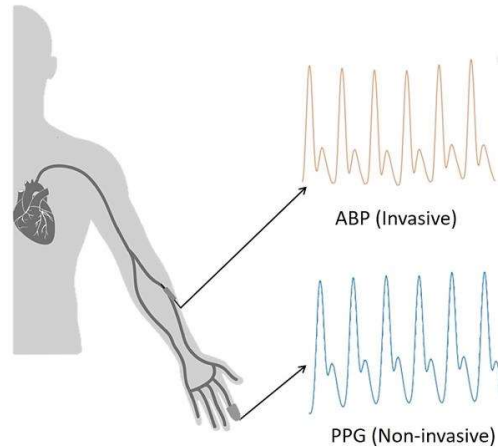


Figure 6. Conventional PPG and ABP measurement method.

It can be observed that the ABP signal is obtained first and then the PPG signal is measured. So, there exists a path difference between obtained ABP and PPG signals which need to be matched for training our model. This phase difference is considered as a lag in signal analysis. The databases contain signals measured with different devices. So, to match the phase difference between the two signal windows, cross-correlation was performed. The location of the maximum value of the cross-correlation indicates a time lag. Keeping the PPG window fixed, the ABP window was shifted by the estimated time lag. The phase-matching process is shown in Figure 7. As the proposed U-net architecture's input size is 256 samples, windows having less than 256 samples were not considered for our experiment, and windows having more than 256 samples were trimmed. The duration of each 256 sample window is 2.048 s.

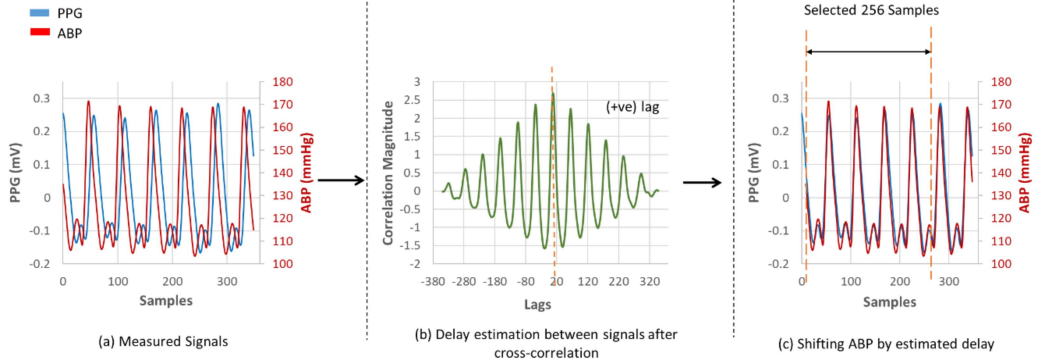


Figure 7. Phase difference matching between PPG and ABP waveforms. (a) Measured Signals; (b) Delay estimation between signals after cross-correlation; (c) Shifting ABP by estimated delay.

### 3.2.4 Normalization

Finally, the obtained data were normalized using Equation (1)

$$x_{norm(i)} = \frac{(x_i - x_{min})}{x_{max} - x_{min}}, \quad (1)$$

where  $x_i$  refers to  $i^{\text{th}}$  signal window, and  $x_{max}$  and  $x_{min}$  are the maximum and minimum values of all the windowed signals, respectively. It is to mention that  $x_{max} = 2.9mV$  and  $x_{min} = -2.4mV$  for PPG and  $x_{max} = 236mmHg$  and  $x_{min} = 20mmHg$  for ABP. The normalized PPG and ABP signal windows were used input and target data for the proposed U-net model.

### 3.2.5 Pre-processed Final Dataset

The preprocessed dataset was distributed widely from lowest to highest SBP and DBP values. Figure 8 illustrates the distribution of SBP and DBP values used for target values in our estimation process. The plots indicate that all SBP and DBP values for all of the four BP ranges are present in our dataset. After final preprocessing, approximately 195 h of data of 100 subjects were achieved. The final dataset contains on average 3.4 h of data for each subject.

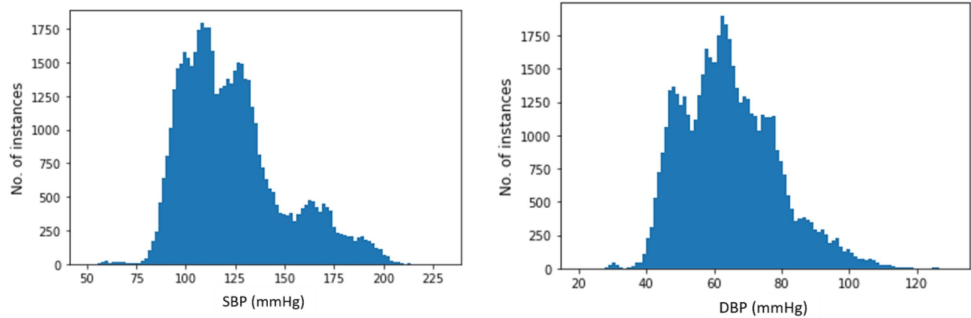


Figure 8. Distribution of SBP and DBP values.

### 3.3 U-net Architecture

Our proposed modified U-net model that predicts the non-invasive ABP signal using the PPG signal as input is shown in Figure 9. U-net uses a fully connected neural network model for semantic segmentation [45]. Inspired by this popular U-net architecture, we proposed a modified U-net model. The network architecture is shaped just like a ‘U’ which justifies the name. This U-net network is consisted of two paths: contracting and expansive path. The contracting path on the left side is made of several contraction blocks (CB) and the expansive path is made of several expansion blocks (EB).

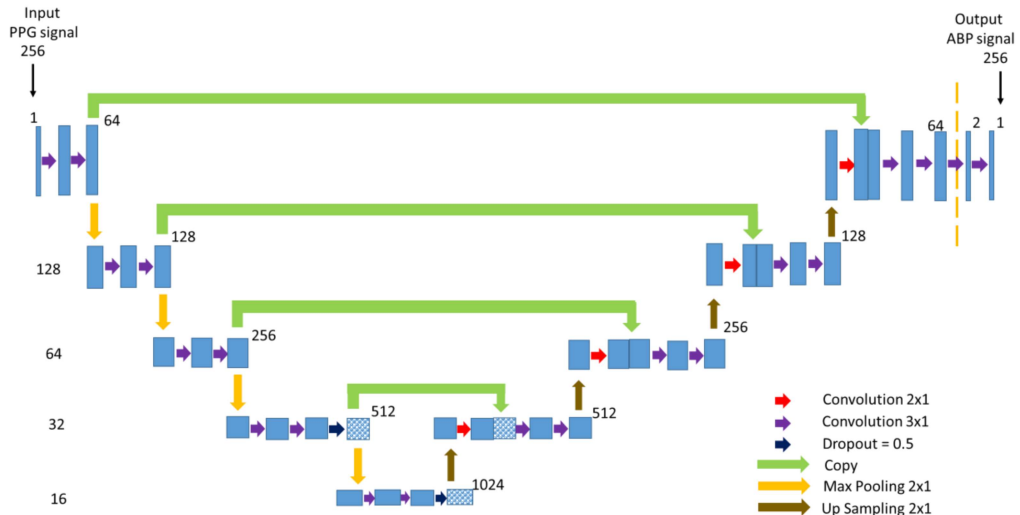


Figure 9. The architecture of the proposed U-net deep learning model.

### 3.3.1 Contracting Path

In Figure 9, the number on the left side of each block denotes the input vector size of that block. As our goal is to predict a properly shaped ABP signal, the input of the network is a PPG signal with a length of 256 samples of 1 dimensional (1D) convolution layer despite being 2 dimensional (2D) as the actual U-net architecture. In our modified network, each block takes an input that applies two  $3 \times 1$  convolution layers followed by a Leaky Rectified Linear Unit (ReLU) activation function after each convolution layer and  $2 \times 1$  max-pooling layer. The Leaky ReLU activation function was used to avoid the dying ReLU problem. The number of feature channels after each block doubles in the contracting path so that the architecture can learn the complicated structures effectively. The number on the upper corner side of a block denotes the number of feature vectors or channels. In the last block of contacting path there is two  $3 \times 1$  convolution layers like before. Dropout of 50% was applied at the last two layers of the contracting path.

### 3.3.2 Expansion Path

The expansion path is symmetric to the contracting path. Each expansion block passes the input to a  $2 \times 1$  up-sampling layer, one  $2 \times 1$  and two  $3 \times 1$  convolution layers followed by a Leaky ReLU activation function after each convolution layer. After each expansion block, the number of feature channels used by the convolutional layer is halved to maintain symmetry. Moreover, the output of the  $2 \times 1$  convolution layer is concatenated with the feature channels from the corresponding contracting path. This action ensures that the features that are learned while contracting the signal will be used to reconstruct it. Finally, at the last expansion path, two extra  $3 \times 1$  convolution layers are used to map each 64 feature vector equal to the input dimension. Using this network, the PPG signal window of 256 samples is mapped into the ABP signal window of 256 samples.

## 3.4 Squeeze U-net Architecture

Inspired from SqueezeNet type of U-net model for biomedical image segmentation has been presented to make it easier to develop deep neural networks on embedded systems while keeping computation and memory needs low, especially for real-time smartphone application. It is called Squeeze U-net [46]. The Squeeze U-net network is proven to be faster in case of training as well as inference than U-net retaining almost similar percentage of accuracy. Deep neural networks are often over parametrized, as evidenced by the fact that a myriad of

compression methods have been applied to vast parameter fields with little or small accuracy loss. Deep learning models with redundant components waste energy and memory. It also increases computational complexity. Several strategies based on factorizability have been proposed to minimize the number of parameters and processing effort for CNNs. Depth-wise convolution [47] a filter channel is used for a input channel only in spite of using direct convolution in the depth dimension like standard convolution. Depth-wise convolution is used in the Squeeze U-net model.

The SqueezeNet fire module [48] architecture in has been used in both the U-net contracting and expansion paths while designing Squeeze U-net. The initial depth-wise convolution of the fire module reduces the number of channels, which is compensated by an starting stage with two parallel convolutions, each of the convolutions with half the number of output channels of that of the fire module. Both of the parallel convolutions support to avoid feature loss and vanishing gradients and feature loss, that can occur when the number of channels is reduced [49].

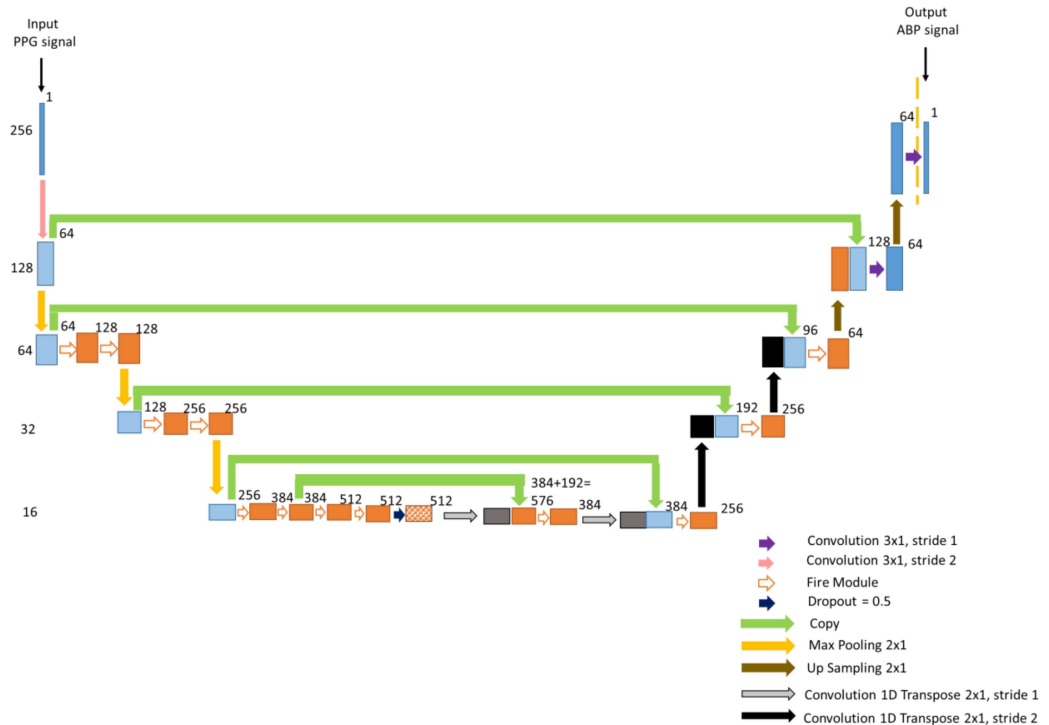


Figure 10. The architecture of Squeeze U-net deep learning model.

The modified Squeeze U-net model is illustrated in Figure 10. Though the number of layers of the proposed Squeeze U-net is more than U-net, the training and inference time for Squeeze U-net is much faster than U-net. Like U-net, it has contacting and expansive path which gives the model a U-shaped structure. Similarly, the model has contracting and expansion path in the left and right side, respectively. The contracting and expansion paths are consisted of several contraction blocks (CB) and expansion blocks (EB) as like as the U-net.

### 3.4.1 Contracting Path

The PPG window of 256 samples used as the input in the contracting path. The input is passed to the  $3 \times 1$  convolution unit with stride 2. Striding helps to down sample and decrease the number of samples to 128 and increase the model's expressiveness. This is the 1<sup>st</sup> block (CB1) of the model. In CB2, the output of the convolution unit (CB1) goes to the  $2 \times 1$  max-pooling layer. No convolution operation is performed in CB2. Max-pooling halves the samples from 128 to 64. The output of the CB2 is passed into two fire modules and one  $2 \times 1$  max-pooling in CB3. In the Squeeze U-net network, fire modules are introduced for down sampling units in the contracting path. The fire modules are used to reduce total parameter number for the model.

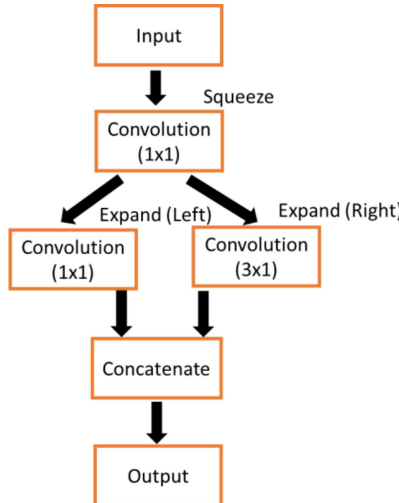


Figure 11. The structure of a fire module of Squeeze U-net.

The structure of a fire module is shown in Figure 11. The fire modules are consisted of a squeeze convolution unit, two expand convolution units and a concatenate unit. The squeeze unit has  $1 \times 1$  convolution filters. The output of this unit goes to expand convolution units of

$1 \times 1$  filters (left) and  $3 \times 1$  filters in parallel (right). Majority of the filters are  $1 \times 1$  because these have fewer number of parameters than  $3 \times 1$  filter. The number of convolution filters in  $1 \times 1$  squeeze unit,  $1 \times 1$  expand unit, and  $3 \times 1$  expand unit are denoted as  $s_{1 \times 1}$ ,  $e_{1 \times 1}$ , and  $e_{3 \times 1}$ , respectively. While using fire modules,  $s_{1 \times 1}$  is set less than  $(e_{1 \times 1} + e_{3 \times 1})$  to limit the number of input samples. In  $3 \times 1$  convolution unit, the total number of parameters is  $(\text{input samples}) * (\text{filters}) * (3 \times 1)$ . So, in CNN, to decrease the number of parameters, it is necessary to minimize the number of input samples. Thus the output of the expand units goes to the concatenate unit to give  $(e_{1 \times 1} + e_{3 \times 1})$  filters. The result of the concatenate unit is the output of the fire module.

The fire modules of CB3 have 16 squeeze filters ( $s_{1 \times 1}$ ) and 64 expand filters ( $e_{1 \times 1}$  and  $e_{3 \times 1}$ ). Then the 4<sup>th</sup> block (CB4) of the contracting path comes, which has similar structure as CB3. The fire modules of CB4 have 32  $s_{1 \times 1}$  and 128  $e_{1 \times 1}$  and  $e_{3 \times 1}$ . The last block (CB5) of the contracting path is max-pooled and passes four fire modules. First two fire modules have 48  $s_{1 \times 1}$  and 192  $e_{1 \times 1}$  and  $e_{3 \times 1}$ . The rest two fire modules have 64  $s_{1 \times 1}$  and 256  $e_{1 \times 1}$  and  $e_{3 \times 1}$ . Then dropout is performed and the output is passed into one-dimensional convolution transpose unit with stride 1. The output of this block is concatenated with the output of the 2<sup>nd</sup> fire module of block CB5. The concatenated output goes to a fire module. This fire module has 48  $s_{1 \times 1}$  and 192  $e_{1 \times 1}$  and  $e_{3 \times 1}$ . The output of this fire module again passed into 2x1 one-dimensional convolution transpose unit with stride 1. The output of this block is concatenated with the input of the fire modules of CB5 and the concatenated result is passed into a fire module. This fire module has 32  $s_{1 \times 1}$  and 128  $e_{1 \times 1}$  and  $e_{3 \times 1}$ . Similar to the structure of U-net, this Squeeze U-net network use Leaky ReLU activation function in every convolution unit.

### 3.4.2 Expansion Path

The expansion path has two  $2 \times 1$  one-dimensional convolution transpose unit with stride 2 followed by two  $2 \times 1$  up sampling units. The output of the convolution transpose units is passed into concatenation units. Every time the number of feature channel is halved to maintain a symmetrical structure to the contracting path. The EB1 and EB2 blocks of expansion path have fire module. The outputs of concatenation blocks go to these fire modules. The fire modules of the expansion block are similarly structures as those of contracting path. The fire module of EB1 of the expansion path has 32  $s_{1 \times 1}$  and 128  $e_{1 \times 1}$  and  $e_{3 \times 1}$  and EB2 has 32  $s_{1 \times 1}$  and 128  $e_{1 \times 1}$  and  $e_{3 \times 1}$ . The output of up sampling unit of EB3 goes to the concatenation unit of EB3. The

output of the concatenated unit passes into a  $3 \times 1$  convolution unit of stride 1 in EB3. The output of the EB3 up sampling unit again passes to  $3 \times 1$  convolution unit in EB4 and give the output ABP window of 256 samples.

### 3.5 ABP Waveform Estimation Process

Using the trained U-net and squeeze U-net model with a PPG signal as an input to the model, we can estimate an ABP waveform. However, note that we trained the model with normalized PPG signals as input and normalized ABP signals as a target. During the ABP waveform estimation process with the test dataset, we need to use a normalized PPG signal as an input and the output data should be de-normalized. While pre-processing the data, the maximum and minimum values of ABP were saved. They were used as de-normalization factors for the estimated ABP waveform.

SBP, DBP, and MAP were also obtained from the ABP waveform. A standard peak and valley detection algorithm [50] was used to detect the SBP and DBP values of estimated ABP signal windows. For each window, the average of SBP and DBP was taken and considered as the SBP and DBP for that individual window. Similarly, the same algorithm was used to calculate the SBP and DBP values from the ABP windows of the reference test dataset. Generally, in invasive blood pressure measurement, SBP and DBP values are calculated from ABP signal. We utilize the same process to estimate SBP and DBP values from reference and predicted ABP signals to see how much these two values correlate with each other. Additionally, MAP values were obtained by calculating the arithmetic mean of every reference and predicted ABP window [51]. Finally, the obtained values from our model were compared with the reference values for result calculation.

## Chapter 4

# Result Evaluation

This result evaluation and discussion chapter will discuss on the estimation result of ABP waveform and measurement result of SBP, DBP and MAP values using U-net and squeeze U-net models. As the topics are diverse, the chapter is will be discussed into several sections. The sections are described sequentially.

### 4.1 Hyper-Parameter and Equipment Setup

We used 70% of the total data for training our model, 15% for validation, and the remaining 15% for testing. The training, validation, and test datasets were completely separated from each other. The training dataset is used for network training and depending on the error, the network is tuned. The validation is performed with the validation dataset for generalizing the network and to stop training when generalization does not improve anymore. The testing provides an independent measurement of the network performance. The model was trained using Adam optimizer and the mean squared error loss function was chosen. The learning rate was set to  $10^{-4}$  and the batch size was selected 4 for U-net and 10 for squeeze U-net model.

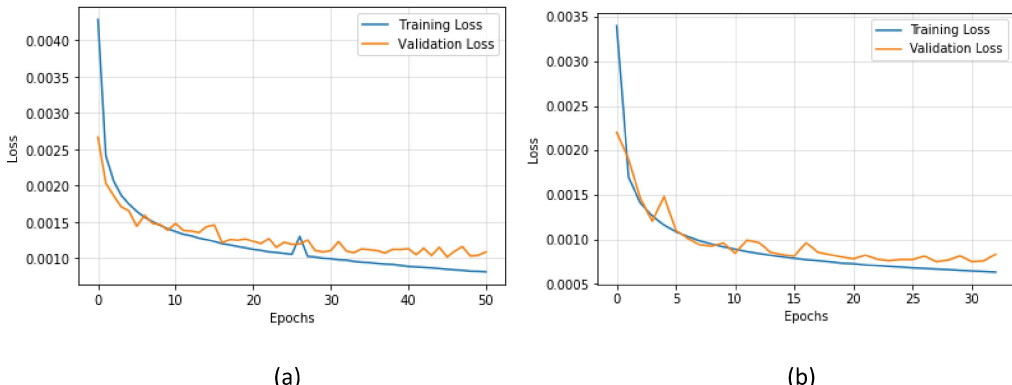


Figure 12. Loss versus epochs curves for (a) U-net and (b) Squeeze U-net model.

The network parameters including the learning rate and batch size were all determined experimentally. Early stopping was used when no improvement was seen in five consecutive epochs and as a result, the training was stopped in 51 epochs for U-net and 33 epochs for squeeze U-net model. Figure 12 shows the training and validation loss versus epochs curves

for U-net and Squeeze U-net, respectively. For each epoch in this training process, the epoch performed in lower validation loss was automatically saved. After the model training procedure was finished, the previously auto-saved model was selected as the final trained model. In our experiment, a GPU server containing NVIDIA GTX 1080 Ti 10 GB graphics card and 257 GB system memory was used. All the codes were written in Python.

## 4.2 Predicted Continuous and Non-Invasive ABP Waveform Analysis Results

The predicted ABP waveforms using our proposed U-net model correlated highly with the reference waveforms. An example of a subject is shown in Figure 13. The reference ABP signal is measured invasive data but phase matched with the input PPG signal. The predicted ABP waveform is almost accurate as the reference ABP signal.

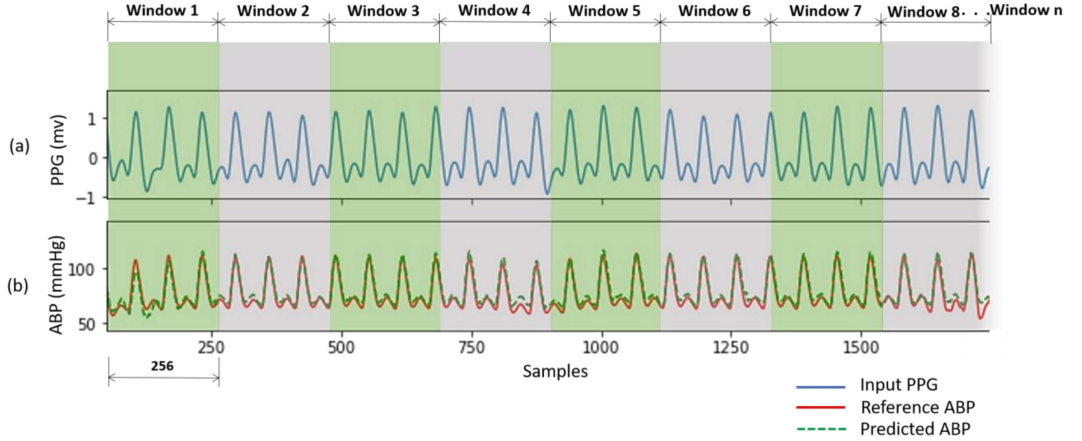


Figure 13. Predicted ABP waveform from PPG of a subject. (a) Input PPG signal; (b) Reference ABP signal and Predicted ABP signal.

To evaluate our obtained ABP waveform result, Pearson's correlation coefficient ( $r$ ) was estimated between the predicted and reference ABP signals as this is used to measure the similarity between two-time series data [40]. The distribution of  $r$  for all the predicted signal windows in the test dataset is shown in Figure 14. Figure 14 shows that most of the values (X-axis) are between 0.9 to 1.0, which depicts high correlation of the predicted ABP signal with the reference signal windows. And from Table 1, the average Person's correlation coefficient ( $r$ ) value can be seen as 0.993. Before calculating the average, we performed Fisher-Z transformation and again performed retransformation after calculating the average to calculate the average  $r$  [52]. Table 1 also gives the value of the maximum and the minimum value of  $r$

for all the windows. The value of the 25<sup>th</sup> and 75<sup>th</sup> percentile of  $r$  says that our proposed U-net model predicted most of the waveform accurately.

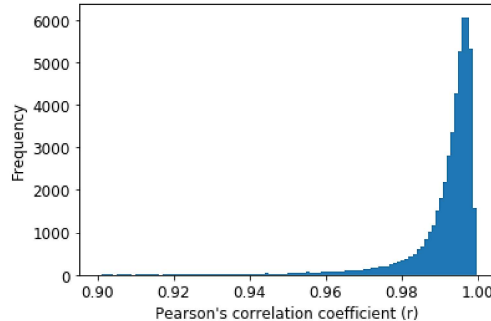


Figure 14. Distribution of Pearson's correlation coefficient.

Table 1. Performance summary of U-net model on test dataset for ABP waveform prediction.

Model	Evaluation Factor	Value
U-net	Average $r$	0.993
	Minimum $r$	0.262
	Maximum $r$	0.999
	25th percentile of $r$	0.989
	75th percentile of $r$	0.996

### 4.3 SBP and DBP Estimation Results

To evaluate our obtained SBP, DBP, and MAP results, mean absolute error (MAE), standard deviation (STD), root mean square error (RMSE), and Pearson's correlation coefficient ( $r$ ) performance metrics were calculated [53].

Table 2. Performance detail of U-net and Squeeze U-net models for SBP, DBP, and MAP values measurement.

Model	Measurement	MAE(mmHg)	STD (mmHg)	RMSE (mmHg)	$r$
U-net	SBP	3.68	4.42	5.75	0.976
	DBP	1.97	2.92	3.52	0.970
	MAP	2.17	3.06	3.75	0.976
Squeeze U-net	SBP	4.42	4.78	6.50	0.970
	DBP	2.25	2.98	3.73	0.964
	MAP	2.56	3.21	4.10	0.971

The performance metrics of our proposed model to estimate SBP, DBP, and MAP values are listed in Table 2. The models predicted DBP values comparatively better than SBP values.

However, in both cases, the values of measurement factors are quite well which denotes that the proposed models can be used to measure SBP, DBP, and MAP easily and accurately. The histograms of the prediction error using the modified U-net and Squeeze U-net models for SBP and DBP values are displayed in Figure 15 and Figure 16.

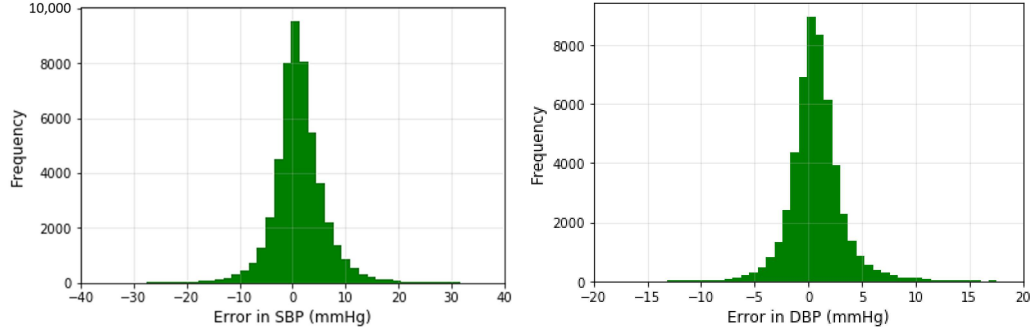


Figure 15. Error histograms of predicted SBP and DBP values using U-net.

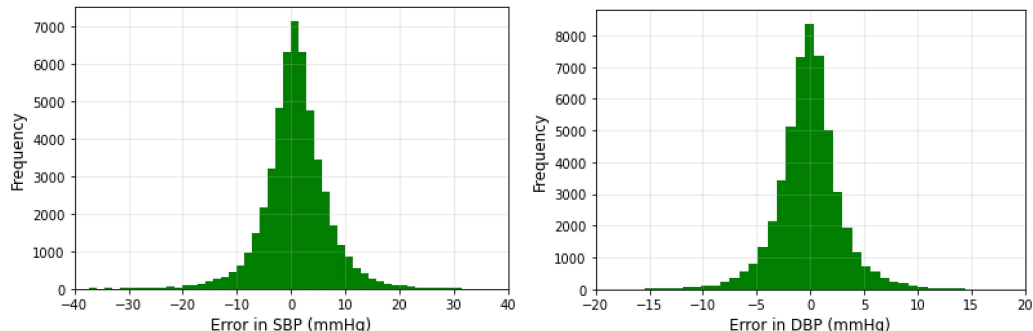


Figure 16. Error histograms of predicted SBP and DBP values using Squeeze U-net.

The error is distributed around zero. According to the histogram, the deviation of the predicted value of SBP is almost twice the DBP value. The result recorded in Table 2 proves the correctness of our observation.

Figure 12 illustrates that the proposed model performs best in the normal BP range. In the normal range, the SBP prediction rate is 97.09% and DBP is 99.04% accurate. In the pre-hypertension range, the prediction of SBP values is better than DBP values for the test dataset. For stage-1 hypertension, the accuracy rate is comparatively low in both cases. In this range, more than 35% of SBP and 22% DBP values deviate more than 10 mmHg. Many values in the range of stage-1 hypertension are identified in the range of pre-hypertension. Though stage-1 hypertension had some deviations in prediction, the prediction rate is quite well for the stage-

2 hypertension range. According to Figure 12, the majority of the values are classified properly using the proposed model. The deviation largely remains within 10 mmHg. For a large quantity of data, very few values are found in more than 20 mmHg deviation area which is negligible.

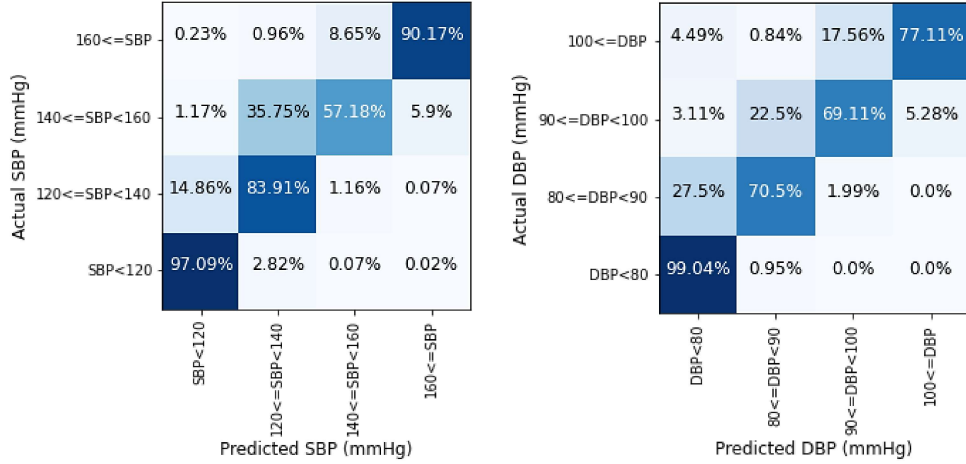


Figure 17. Prediction accuracy of SBP and DBP values in four BP ranges using U-net.

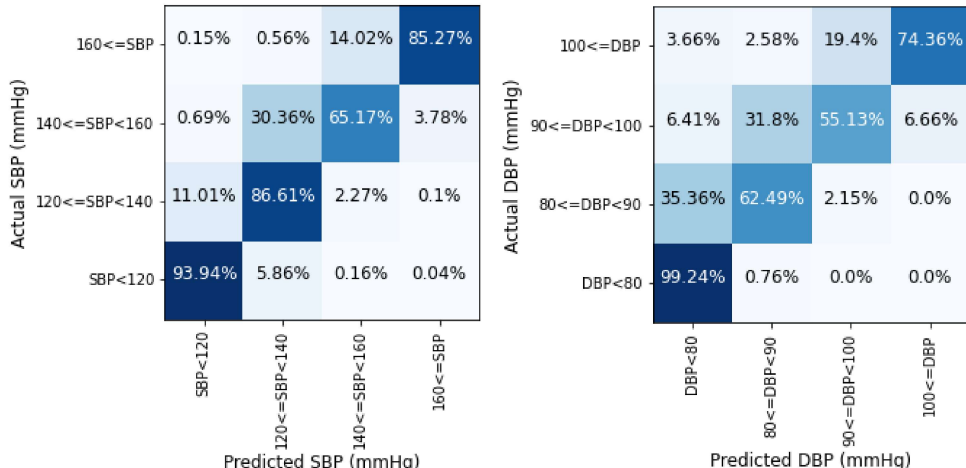


Figure 18. Prediction accuracy of SBP and DBP values in four BP ranges using Squeeze U-net.

The scatter plots of our predicted result with respect to the actual SBP, DBP, and MAP are shown in Figure 19 and Figure 20 for U-net and Squeeze U-net, respectively. It is shown that the obtained result gives a linear correlation, which proves that the predicted result is mostly accurate except in very few cases.

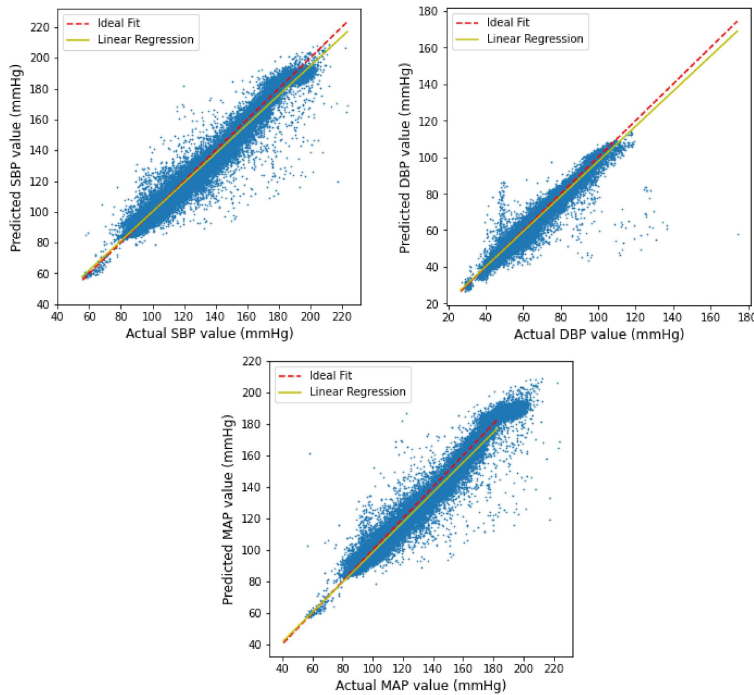


Figure 19. Linear regression plot of the SBP, DBP, and MAP result using U-net.

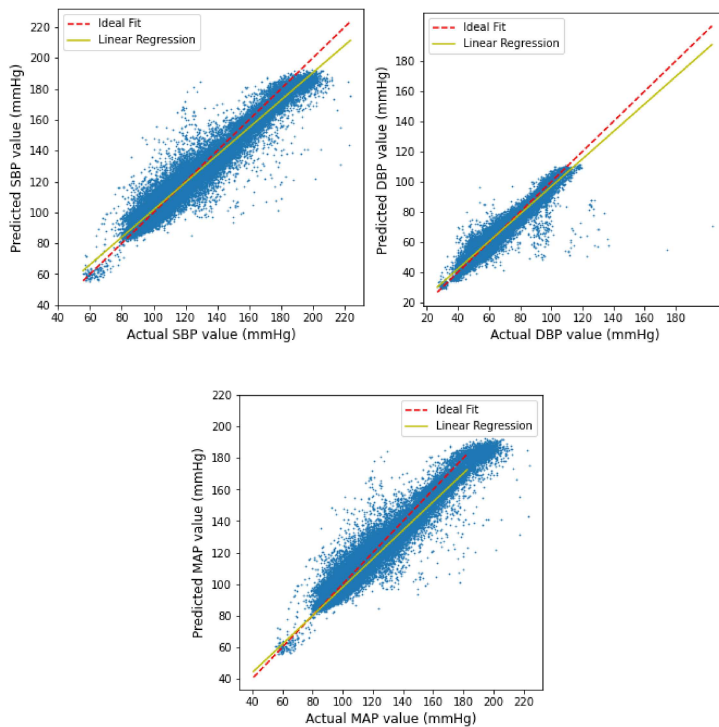


Figure 20. Linear regression plot of the SBP, DBP, and MAP result using Squeeze U-net.

The Bland-Altman plots for the proposed algorithm are displayed in Figure 14 maintaining the AAMI criteria [54]. The x-axes represent pressure from 80 to 190 mmHg for SBP and 30 to 140 mmHg for DBP. The y-axes denote errors in the range of  $-30$  to  $+30$  mmHg. Reference horizontal dotted lines are shown at the interval of 5 mmHg from  $-15$  to  $+15$  mmHg. The mean of each actual BP and its relative predicted BP is plotted across their difference with a point. Greater than 30 mmHg differences are plotted at 30 mmHg and less than  $-30$  mmHg are plotted at  $-30$  mmHg. It is observed that most of the SBP and DBP errors lie between  $-5$  to  $5$  mmHg in both cases.

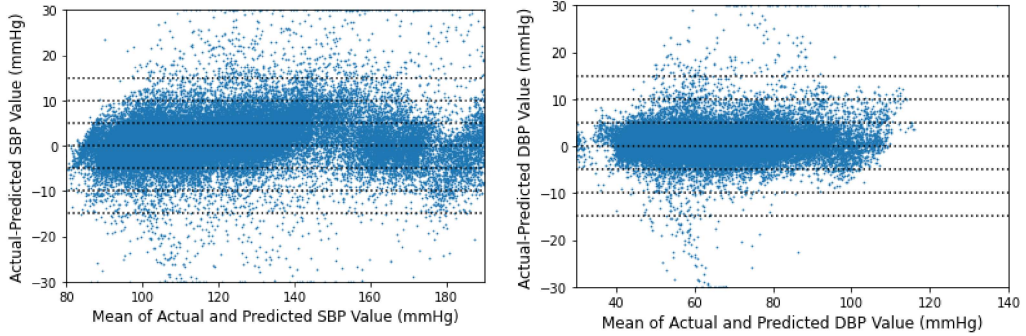


Figure 21. Bland-Altman scatterplot for predicted SBP and DBP values using U-net.

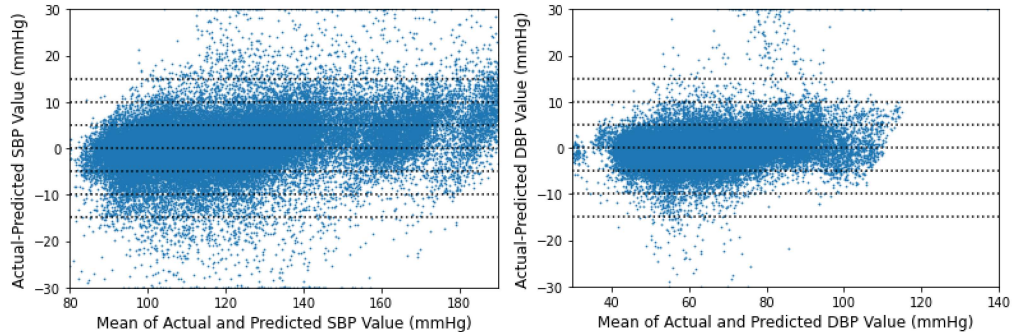


Figure 22. Bland-Altman scatterplot for predicted SBP and DBP values using Squeeze U-net.

#### 4.4 Compliance with Standards

The obtained result was compared with the AAMI error range. According to AAMI, the mean difference and standard deviation must be less than or equal to  $5 \pm 8$  mmHg [55]. The predictions of our modified U-net and Squeeze U-net network are fully acceptable for SBP and DBP values. The comparison with the AAMI standard is shown in Table 3.

Table 3. Comparison of our result with the Association for the Advancement of Medical Instrumentation (AAMI) standard.

		No. of Subjects	MAE (mmHg)	STD (mmHg)
AAMI [44]	BP	> 85	≤ 5	≤ 8
U-net	SBP	100	3.68	4.42
	DBP		1.97	2.92
Squeeze U-net	SBP	100	4.42	4.78
	DBP		2.25	2.98

The accuracy of the model is also checked from the point of view of the British Hypertension Society (BHS) grading standard [56]. The BHS grading standard and the cumulative error percentage of our data are shown in Table 4. According to the result, it can be said that the estimation of SBP and DBP using our model fall in the “Grade A”.

Table 4. Comparison of the result with British Hypertension Society (BHS) grading standard.

BHS grading standard [45]		Cumulative Error (%)		
		≤ 5 mmHg	≤ 10 mmHg	≤ 15 mmHg
		Grade A	60%	85%
		Grade B	50%	75%
U-net	SBP	76.21%	93.66%	97.71%
	DBP	93.51%	98.70%	99.46%
Squeeze U-net	SBP	64.20%	87.85%	95.26%
	DBP	95.58%	99.35%	99.67%

#### 4.5 Comparison Between U-net and Squeeze U-net Models

Table 5. Comparison of the number of U-net and Squeeze U-net parameters in contraction path.

Block Name	Squeeze U-net		U-net		Reduction Factor
	Layer Size	#Params	Layer Size	#Params	
CB1	[3 × 1 × 64]	256	[3 × 1 × 64] × 2	12608	49.3×
CB2	--	0	[3 × 1 × 28] × 2	73984	--
CB3	$\begin{bmatrix} 1 \times 1 \times 16 \\ 1 \times 1 \times 64 \\ 3 \times 1 \times 64 \end{bmatrix} \times 2$	11680	[3 × 1 × 256] × 2	295424	25.3×
CB4	$\begin{bmatrix} 1 \times 1 \times 32 \\ 1 \times 1 \times 128 \\ 3 \times 1 \times 128 \end{bmatrix} \times 2$	45888	[3 × 1 × 512] × 2	1180672	25.7×

CB5	$\begin{bmatrix} 1 \times 1 \times 48 \\ 1 \times 1 \times 192 \\ 3 \times 1 \times 192 \end{bmatrix} \times 2$	105696	$[3 \times 1 \times 1024] \times 2$	4720640	6.9×
	$\begin{bmatrix} 1 \times 1 \times 64 \\ 1 \times 1 \times 256 \\ 3 \times 1 \times 256 \end{bmatrix} \times 2$	190080			
	$[2 \times 1 \times 192]$	196800			
	$\begin{bmatrix} 1 \times 1 \times 48 \\ 1 \times 1 \times 192 \\ 3 \times 1 \times 192 \end{bmatrix}$	65136			
	$[2 \times 1 \times 128]$	98432			
	$\begin{bmatrix} 1 \times 1 \times 32 \\ 1 \times 1 \times 128 \\ 3 \times 1 \times 128 \end{bmatrix}$	29088			
<b>Total</b>		<b>743056</b>		<b>6283328</b>	<b>8.5×</b>

Table 6. Comparison of the number of U-net and Squeeze U-net parameters in Expansion path.

Block Name	Squeeze U-net		U-net		Reduction Factor
	Layer Size	#Params	Layer Size	#Params	
EB1	$[2 \times 1 \times 64]$	8224	$[2 \times 1 \times 512]$	1049088	285.3×
	$\begin{bmatrix} 1 \times 1 \times 16 \\ 1 \times 1 \times 64 \\ 3 \times 1 \times 64 \end{bmatrix}$	3728	$[3 \times 1 \times 512] \times 2$	2360320	
EB2	$[2 \times 1 \times 32]$	32832	$[2 \times 1 \times 256]$	262400	21.2×
	$\begin{bmatrix} 1 \times 1 \times 16 \\ 1 \times 1 \times 32 \\ 3 \times 1 \times 32 \end{bmatrix}$	7376	$[3 \times 1 \times 256] \times 2$	590336	
EB3	$[3 \times 1 \times 64]$	24640	$[2 \times 1 \times 128]$	65665	8.7×
			$[3 \times 1 \times 128] \times 2$	147712	
EB4	$[3 \times 1 \times 1]$	65	$[2 \times 1 \times 64]$	16448	828.2×
			$[3 \times 1 \times 64] \times 2$	36992	
			$[3 \times 1 \times 2]$	386	
			$[3 \times 1 \times 3]$	7	
<b>Total</b>		<b>76865</b>		<b>4529354</b>	<b>58.9×</b>

Comparison of the number of parameters between U-net and Squeeze U-net in contracting path and expansion path is given in Table 5 and Table 6, respectively. The tables show that in every block of contracting path and expansion path, huge reduction factor is observed in the number of parameters. It denotes that Squeeze U-net model works almost similar as U-net model with reduced number of parameters.

Table 7. Quantitate comparison between U-net and Squeeze U-net regarding model size, number of operations and prediction time.

Model	Size (MB)	#Float Operations	Time/Prediction (ms)
U-net	126.91	162176642	2.00
Squeeze U-net	101.44	1637678	0.32
Reduction Factor	1.3 $\times$	99 $\times$	6.1 $\times$

Furthermore, quantitate comparison of the models is based on model size, number of floating point operations, and per signal window prediction time is shown in Table 7. The result shows that size of Squeeze U-net model is 1.3 $\times$  times smaller than U-net. The number of floating point operations is 99 $\times$  times and per signal window prediction time is 6.1 $\times$  times lesser than U-net model. It proves that Squeeze U-net can be computationally very effective for smart devices.

#### 4.6 Comparison with Related Works

In general, it is difficult to compare related works due to different evaluation metrics, and the difference in datasets. However, to compare properly, we considered MAE, STD, RMSE, and r as comparison factors. Table 8 summarizes the performance of our proposed method with other related works.

Reviewing other related works, we found authors of [32] used a similar dataset similar to our experiment. But there was inconsistency in their data which is described in our related works section.

In [33], a very small subset of the Queensland Vital sign dataset was used. The work in [29] and [36] prepared their own dataset which is not publicly available. In [29], two subject-specific parameters were also used to calibrate the data, which will vary for different subjects.

However, the studies of [28] and [58] used the publicly available MIMIC-II database. But [28] needed two signals (ECG and PPG) and several features to estimate BP. And on the other hand, our model obtained comparatively better MAE and STD than [58]. In [33] and [57], the total amount of data was also very small and the result was also not satisfactory. Moreover, the work of [28], [32], [33], [36], and [58] needed beat segmentation to detect single PPG cycles.

Table 8. Result comparison with related works.

Method	Dataset	Source	Data Used for Test	Prediction	SBP DBP			
					MAE	STD	RMSE	r
					(mmHg)			
Squeeze U-net	MIMIC I, MIMIC III waveform	PPG (raw)	29.3 h	SBP, DBP, and MAP waveform	4.42  2.25	4.78  2.98	6.50  3.73	0.97  0.96
Modified U-net	MIMIC I, MIMIC III waveform	PPG (raw)	29.3 h	SBP, DBP, MAP, and ABP waveform	3.68  1.97	4.42  2.92	5.75  3.52	0.97  0.97
ANN [32]	MIMIC I	PPG (feature)	8819 single PPG	SBP and DBP	4.02  2.27	2.79  1.82	--	--
Random Forest (RF) [33]	Queensland Vital Signs	PPG (feature)	2298 single PPG	SBP and DBP	4.21  3.24	7.59  5.39	7.57  5.40	0.93  0.94
CNN [36]	Self-made	PPG (raw)	50000 single PPG	SBP and DBP	--	11.4	--	0.71
PTT [29]	Self-made	SCG, PPG	--	SBP and DBP	--	--	4.8  2.9	--
Long short-term memory (LSTM) [28]	MIMIC II	PPG, ECG (feature)	135641 PPG and ECG cycles	SBP, DBP, and MAP	4.63  3.15	14.50  6.44	--	--
Machine Learning [57]	Self-made, Physionet	ECG (feature)	7.8 h	SBP, DBP, and MAP	7.72  9.45	--	--	--
ResNet-GRU [34]	MIMIC III Waveform	PPG (raw)	140 h	SBP and DBP	9.43  6.88	--	--	--
CNN and LSTM [58]	MIMIC II	PPG (raw)	103760 single PPG	SBP and DBP	3.97  2.10	5.55  2.84	--	0.95  0.95

Another work in [34] used waveforms of a huge MIMIC III database. Though they claimed their model could predict regular BP for home use, the result didn't meet the requirement of the AAMI standard error range.

Compared to the described approaches, our method obtained better accuracy for SBP and DBP values. So our proposed technique can be confidently adopted as the SBP and DBP estimation technique for regularly using devices. Moreover, our proposed U-net model is the only model that can predict the very informative ABP waveform. To the best of our knowledge, no other models have predicted ABP waveform using the raw PPG signal so far.

As the dataset and pre-processing techniques varies in the above mentioned methods, we implemented the models of [32]–[34], [36]. We trained and tested the models using our pre-processed data and we used pre-processed PPG signals as the only input. The obtained result is stated in Table 9.

Table 9. Comparison with related works using our pre-processed PPG signal.

Method	SBP DBP			
	MAE (mmHg)	STD (mmHg)	RMSE (mmHg)	r
Squeeze U-net	4.42  2.25	4.78  2.98	6.50  3.73	0.97  0.96
Modified U-net	3.68  1.97	4.42  2.92	5.75  3.52	0.97  0.97
ANN [32]	18.34  9.98	15.02  7.78	23.71  12.65	0.30  0.49
Random Forest (RF) [33]	13.14  6.77	12.38  6.30	18.05  9.25	0.72  0.79
ResNet-GRU [34]	7.78  5.32	7.79  4.67	11.15  7.08	0.89  0.88
CNN [36]	14.41  7.59	13.45  6.59	19.71  10.05	0.64  0.73

The comparison with related works that used only PPG signal using a small subset of our pre-processed PPG signal is shown in Table 9. Except our two models (U-net and Squeeze U-net), only SBP and DBP values have been predicted using all the other models. The result shows that using same data the result of our proposed models is better than other models.

Table 10. Quantitative comparison among Squeeze U-net model with related works.

Method	#Params	Time/ Prediction (ms)
Squeeze U-net	819,921	0.32
ANN [32]	98,946	0.04
Random Forest (RF) [33]	100 estimators	19.02
ResNet-GRU [34]	264,688	4.00
CNN [36]	2,164,738	0.09

Table 10 shows the number of parameters and prediction time for SBP and DBP values per window using different models with the same data. The parameter number is less in [32]–[34] and higher in [36] than proposed Squeeze U-net model. But the prediction time is longer in [33], [34]. The model in [34] also takes very long time to train and to converge. Both the prediction time and number of parameters are less in [32] than the Squeeze U-net model, but the accuracy is very low as shown in Table 9. The overall performance is better in the proposed Squeeze U-net model with the number of parameters and prediction time. Though the prediction time and number of parameters are not lowest for the chosen Squeeze U-net model, the value is comparatively in the lower side than other models in case of prediction time. We are considering the highest prediction accuracy for ABP waveform, SBP, DBP, and MAP values. Among all the models the Squeeze U-net model shows a balanced performance. Furthermore, it is to mention that only the proposed Squeeze U-net can predict the ABP waveform. Other models of the related works only predicted the SBP and DBP values.

## Chapter 5

# Application Development

In modern times, a wrist watch based or mobile-friendly reliable blood pressure measurement technique is needed to estimate blood pressure value regularly for healthy lifestyle. So, the proposed Squeeze U-net model is used to build an android application to measure mostly needed SBP and DBP values. We named the application “BP Calculator”. This chapter discusses on the process of using this application along with the advantages and the disadvantages of the application.

### 5.1 BP Calculator

Mobile health diagnosis has been proved to be successful and scalable in the identification and management of chronic diseases. By utilizing the optics and computational power of smartphones, they may be able to assess physiological information from the shape of pulse waves and hence estimate blood pressure without using cuff.

Keeping this in mind, the computationally efficient Squeeze U-net model has been used to calculate the BP using an android application named “BP Calculator”. All the stages of prior signal processing are performed in android studio platform. The pre-trained Squeeze U-net model is loaded using TensorFlow Lite. This model is used to predict SBP and DBP values for new subjects.

This could be a useful tool for detecting hypertension in a variety of circumstances, such as low-income nations, where smartphones are widely available but access to health care is limited, can have access to this application without any cost. The preliminary target of this application is for home use.

### 5.2 BP Measurement Process

The step by step blood pressure measurement process using “BP Calculator” application is shown in the Figure 23. By placing the index finger lightly on the camera, the PPG signal is acquired using the rear camera of the smartphone. A person needs to place the finger only for 20 seconds to see the BP values. To get accurate measurement results, the finger or camera cannot be moved until the measurement is completed. After completing the measurement, the SBP and DBP values are shown.

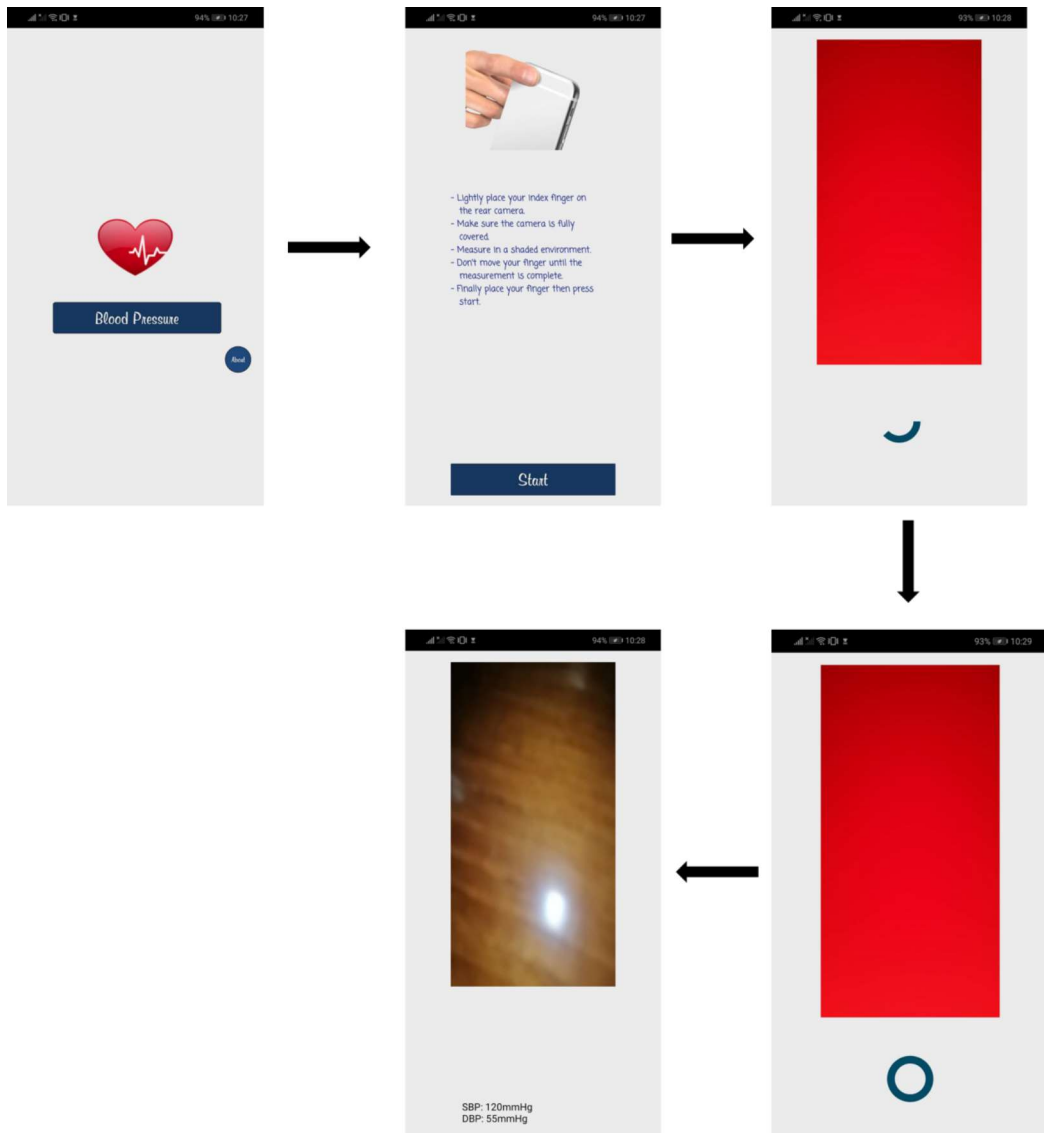


Figure 23. Blood pressure measurement process using “BP Calculator” application.

### 5.3 Advantages of BP Calculator

- A smartphone based BP measurement system is new.
- People can measure BP without any cost.
- BP can be measured regularly in any situation.
- BP can be measured in a short time.
- Hypertension can be detected at early stage.

## 5.4 Disadvantages of BP Calculator

- The acquired PPG signals are extremely sensitive to artifacts due to hand movements, finger pressure and external noises. This may give inaccurate results.
- The PPG signal quality needs to be really good to get accurate BP value.
- Appropriate signal quality checking is needed for the application.
- Not suitable for people with weak PPG signal.
- Not suitable for critical patients.

## Chapter 6

### Discussion and Conclusion

#### 6.1 Discussion

In recent times, a mobile-friendly or wrist watch based reliable BP measurement method is needed to measure BP regularly for a healthy life. So, the proposed Squeeze U-net model using the “BP Calculator” application can be used to measure non-invasive SBP and DBP values easily using smartphones. Moreover, U-net model can be used to estimate the ABP waveforms of critical patients if stable PPG signal is acquired. We focus on estimating the waveform because it is efficient for a 1D-CNN-based model to optimize for a signal target rather than a feature target when the input is a signal. Mainly, the proposed method can be applied for regular use in the current state. It is to be noted that, PPG signals contain different artifacts and the signals are very sensitive to movements, finger pressure, thickness and coloration of the skin, and the nature of the subcutaneous tissue e.g., lots of facts on the fingers. So, this proposed method can be used to monitor the BP of ICU patients if stable PPG signals can be taken using constant pressure on fingertips. However, the problem of artifacts can be overcome. If the detection apparatus is placed at a different location, for example, over the radial and/or ulnar arteries at the wrist, and the patient is instructed to rest and not move the wrist, then appropriate low noise recordings could be obtained.

Next, the performance of the deep learning model strongly depends on the quality and amount of data. The reference ABP waveforms of the databases are measured in the brachial artery. But, our proposed U-net model predicts ABP waveforms from fingertip PPG signal, and this PPG signal is obtained from a digital artery as shown in Figure 1. The predicted ABP waveform is phase-matched with the input fingertip PPG signal as we described before. So, if a person's ABP waveform is measured from the brachial artery as well as from the digital artery using our system at the same time, then there will be little phase difference between the two signals.

## 6.2 Future Research Opportunities

In future studies, there is an opportunity for more research to develop a device that will take stable PPG signals with constant pressure for every critical patient so that it can replace invasive ABP measurement in ICU. A real-time algorithm can be implemented for the android application to measure SBP and DBP values continuously in real-time. Moreover, a real clinical issue is the changes in BP. In the ICU sudden rises or falls in BP are of concern and immediate detection is highly desirable. A prospective study in an ICU can be conducted for checking the sensitivity of changes in BP, particularly wide excursions.

## 6.3 Conclusion

Continuous, non-invasive, and cuff-less comfortable BP measurement technique is a highly researched topic of the current time, to fight against hypertension. Hypertension is the main cause of several heart-related issues. The development of methods to estimate ABP waveform along with SBP, DBP, and MAP values is a promising yet challenging field. The increasing demand for PPG-based applications and wearable devices can provide an interesting direction in this field as PPG-based technology offers both non-invasive and continuous measurement. Keeping that in mind, our research proposed a U-net deep neural network-based continuous and non-invasive ABP waveform estimation method. Moreover, the modified Squeeze U-net model is computationally efficient with almost similar accuracy as U-net model. The “BP Calculator” build with using this compressed model can predict SBP and DBP values at any time without any cost and detect possible hypertension-based bodily issues at early stages. Our U-net model gives continuous and non-invasive ABP waveforms that are highly correlated with the reference invasive ABP signals. Moreover, the obtained SBP and DBP values from the predicted ABP waveforms satisfy the AAMI and BHS standard. We believe, our work can provide a possible solution in the non-invasive, cuffless, continuous measurement methods of BP estimation and assist in keeping BP under control.

## References

- [1] M.-C. Irigoyen, K. De Angelis, F. dos Santos, D. R. Dartora, B. Rodrigues, and F. M. Consolim-Colombo, “Hypertension, Blood Pressure Variability, and Target Organ Lesion,” *Curr Hypertens Rep*, vol. 18, no. 4, p. 31, Mar. 2016, doi: 10.1007/s11906-016-0642-9.
- [2] “Stroke and hypertension,” *World Heart Federation*. <https://www.world-heart-federation.org/resources/stroke-and-hypertension/> (accessed Feb. 06, 2020).
- [3] A. L. Siu, “Screening for High Blood Pressure in Adults: U.S. Preventive Services Task Force Recommendation Statement,” *Ann Intern Med*, vol. 163, no. 10, p. 778, Nov. 2015, doi: 10.7326/M15-2223.
- [4] P. Schoettker *et al.*, “Blood pressure measurements with the OptiBP smartphone app validated against reference auscultatory measurements,” *Scientific Reports*, vol. 10, no. 1, Art. no. 1, Oct. 2020, doi: 10.1038/s41598-020-74955-4.
- [5] J. S. Shahoud and N. R. Aeddula, “Physiology, Arterial Pressure Regulation,” in *StatPearls*, Treasure Island (FL): StatPearls Publishing, 2019. Accessed: Jan. 13, 2020. [Online]. Available: <http://www.ncbi.nlm.nih.gov/books/NBK538509/>
- [6] D. I. Moxham, “Understanding Arterial Pressure Waveforms,” *Southern African Journal of Anaesthesia and Analgesia*, vol. 9, no. 1, pp. 40–42, Feb. 2003, doi: 10.1080/22201173.2003.10872991.
- [7] T. G. Papaioannou *et al.*, “Mean arterial pressure values calculated using seven different methods and their associations with target organ deterioration in a single-center study of 1878 individuals,” *Hypertension Research*, vol. 39, no. 9, Art. no. 9, Sep. 2016, doi: 10.1038/hr.2016.41.
- [8] O. Mf, “Arterial pressure waveforms in hypertension.,” *Minerva Med*, vol. 94, no. 4, pp. 229–250, Aug. 2003.
- [9] R. Velik, “An objective review of the technological developments for radial pulse diagnosis in Traditional Chinese Medicine,” *European Journal of Integrative Medicine*, vol. 7, no. 4, pp. 321–331, Aug. 2015, doi: 10.1016/j.eujim.2015.06.006.
- [10] R. Mukkamala, A. T. Reisner, H. M. Hojman, R. G. Mark, and R. J. Cohen, “Continuous cardiac output monitoring by peripheral blood pressure waveform analysis,” in *Computers in Cardiology*, 2003, Sep. 2003, pp. 255–258. doi: 10.1109/CIC.2003.1291139.

- [11] M. P. M. Harms *et al.*, “Continuous stroke volume monitoring by modelling flow from non-invasive measurement of arterial pressure in humans under orthostatic stress,” *Clinical Science*, vol. 97, no. 3, pp. 291–301, Jul. 1999, doi: 10.1042/cs0970291.
- [12] A. V. Chobanian *et al.*, “The Seventh Report of the Joint National Committee on Prevention, Detection, Evaluation, and Treatment of High Blood Pressure: The JNC 7 Report,” *JAMA*, vol. 289, no. 19, pp. 2560–2571, May 2003, doi: 10.1001/jama.289.19.2560.
- [13] K. B. Siaron, M. X. Cortes, S. E. Stutzman, A. Venkatachalam, K. M. Ahmed, and D. M. Olson, “Blood Pressure measurements are site dependent in a cohort of patients with neurological illness,” *Scientific Reports*, vol. 10, no. 1, Art. no. 1, Feb. 2020, doi: 10.1038/s41598-020-60414-7.
- [14] T. Athaya and S. Choi, “Evaluation of Different Machine Learning Models for Photoplethysmogram Signal Artifact Detection,” in *2020 International Conference on Information and Communication Technology Convergence (ICTC)*, Oct. 2020, pp. 1206–1208. doi: 10.1109/ICTC49870.2020.9289366.
- [15] T. Athaya and S. Choi, “An Estimation Method of Continuous Non-Invasive Arterial Blood Pressure Waveform Using Photoplethysmography: A U-Net Architecture-Based Approach,” *Sensors*, vol. 21, no. 5, Art. no. 5, Jan. 2021, doi: 10.3390/s21051867.
- [16] J. Allen, “Photoplethysmography and its application in clinical physiological measurement,” *Physiol Meas*, vol. 28, no. 3, pp. R1–39, Mar. 2007, doi: 10.1088/0967-3334/28/3/R01.
- [17] K. H. C. Li *et al.*, “The Current State of Mobile Phone Apps for Monitoring Heart Rate, Heart Rate Variability, and Atrial Fibrillation: Narrative Review,” *JMIR mHealth and uHealth*, vol. 7, no. 2, p. e11606, Feb. 2019, doi: 10.2196/11606.
- [18] Mills Katherine T. *et al.*, “Global Disparities of Hypertension Prevalence and Control,” *Circulation*, vol. 134, no. 6, pp. 441–450, Aug. 2016, doi: 10.1161/CIRCULATIONAHA.115.018912.
- [19] B. Zhou *et al.*, “Long-term and recent trends in hypertension awareness, treatment, and control in 12 high-income countries: an analysis of 123 nationally representative surveys,” *The Lancet*, vol. 394, no. 10199, pp. 639–651, Aug. 2019, doi: 10.1016/S0140-6736(19)31145-6.
- [20] J. Špinar, “Hypertension and ischemic heart disease,” *Cor et Vasa*, vol. 54, no. 6, pp. e433–e438, Nov. 2012, doi: 10.1016/j.crvasa.2012.11.002.

- [21] G. Martínez, N. Howard, D. Abbott, K. Lim, R. Ward, and M. Elgendi, “Can Photoplethysmography Replace Arterial Blood Pressure in the Assessment of Blood Pressure?,” *J Clin Med*, vol. 7, no. 10, Sep. 2018, doi: 10.3390/jcm7100316.
- [22] T. Abhay, K. N., and R. G. J., “Estimating Correlation between Arterial Blood Pressure and Photoplethysmograph,” in *16th International Conference on Biomedical Engineering*, Singapore, 2017, pp. 47–52. doi: 10.1007/978-981-10-4220-1\_10.
- [23] G. Tusman *et al.*, “Photoplethysmographic characterization of vascular tone mediated changes in arterial pressure: an observational study,” *J Clin Monit Comput*, vol. 33, no. 5, pp. 815–824, Oct. 2019, doi: 10.1007/s10877-018-0235-z.
- [24] J. Fortin *et al.*, “Continuous non-invasive blood pressure monitoring using concentrically interlocking control loops,” *Computers in Biology and Medicine*, vol. 36, no. 9, pp. 941–957, Sep. 2006, doi: 10.1016/j.combiomed.2005.04.003.
- [25] G. M. Drzewiecki, J. Melbin, and A. Noordergraaf, “Arterial tonometry: review and analysis,” *J Biomech*, vol. 16, no. 2, pp. 141–152, 1983, doi: 10.1016/0021-9290(83)90037-4.
- [26] B. M. Weiss, D. R. Spahn, H. Rahmig, R. Rohling, and T. Pasch, “Radial artery tonometry: moderately accurate but unpredictable technique of continuous non-invasive arterial pressure measurement,” *British Journal of Anaesthesia*, vol. 76, no. 3, pp. 405–411, Mar. 1996, doi: 10.1093/bja/76.3.405.
- [27] M. F. O’Rourke, “Carotid Artery Tonometry: Pros and Cons,” *American Journal of Hypertension*, vol. 29, no. 3, pp. 296–298, Mar. 2016, doi: 10.1093/ajh/hpv194.
- [28] Y.-H. Li, L. N. Harfiya, K. Purwandari, and Y.-D. Lin, “Real-Time Cuffless Continuous Blood Pressure Estimation Using Deep Learning Model,” *Sensors*, vol. 20, no. 19, Art. no. 19, Jan. 2020, doi: 10.3390/s20195606.
- [29] A. M. Carek, J. Conant, A. Joshi, H. Kang, and O. T. Inan, “SeismoWatch: Wearable Cuffless Blood Pressure Monitoring Using Pulse Transit Time,” *Proceedings of the ACM on interactive, mobile, wearable and ubiquitous technologies*, vol. 1, no. 3, Sep. 2017, doi: 10.1145/3130905.
- [30] C.-S. Kim, A. M. Carek, R. Mukkamala, O. T. Inan, and J.-O. Hahn, “Ballistocardiogram as Proximal Timing Reference for Pulse Transit Time Measurement: Potential for Cuffless Blood Pressure Monitoring,” *IEEE Trans Biomed Eng*, vol. 62, no. 11, pp. 2657–2664, Nov. 2015, doi: 10.1109/TBME.2015.2440291.

- [31] Z. Chen, S. H. Ng, J. T. Teo, and X. Yang, “Method and system for optical blood pressure monitoring,” US20150018637A1, Jan. 15, 2015 Accessed: May 18, 2021. [Online]. Available: <https://patents.google.com/patent/US20150018637A1/en>
- [32] L. Wang, W. Zhou, Y. Xing, and X. Zhou, “A Novel Neural Network Model for Blood Pressure Estimation Using Photoplethysmography without Electrocardiogram,” *Journal of Healthcare Engineering*, vol. 2018, p. e7804243, Mar. 2018, doi: <https://doi.org/10.1155/2018/7804243>.
- [33] Q. Xie, G. Wang, Z. Peng, and Y. Lian, “Machine Learning Methods for Real-Time Blood Pressure Measurement Based on Photoplethysmography,” in *2018 IEEE 23rd International Conference on Digital Signal Processing (DSP)*, Nov. 2018, pp. 1–5. doi: 10.1109/ICDSP.2018.8631690.
- [34] G. Slapničar, N. Mlakar, and M. Luštrek, “Blood Pressure Estimation from Photoplethysmogram Using a Spectro-Temporal Deep Neural Network,” *Sensors (Basel)*, vol. 19, no. 15, Aug. 2019, doi: 10.3390/s19153420.
- [35] X. Wang, J. Xu, W. Shi, and J. Liu, “OGRU: An Optimized Gated Recurrent Unit Neural Network,” *J. Phys.: Conf. Ser.*, vol. 1325, p. 012089, Oct. 2019, doi: 10.1088/1742-6596/1325/1/012089.
- [36] S. Shimazaki, H. Kawanaka, H. Ishikawa, K. Inoue, and K. Oguri, “Cuffless Blood Pressure Estimation from only the Waveform of Photoplethysmography using CNN,” in *2019 41st Annual International Conference of the IEEE Engineering in Medicine and Biology Society (EMBC)*, Jul. 2019, pp. 5042–5045. doi: 10.1109/EMBC.2019.8856706.
- [37] M. Radha *et al.*, “Estimating blood pressure trends and the nocturnal dip from photoplethysmography,” *Physiol. Meas.*, vol. 40, no. 2, p. 025006, 26 2019, doi: 10.1088/1361-6579/ab030e.
- [38] C. Holz and E. J. Wang, “Glabella: Continuously Sensing Blood Pressure Behavior using an Unobtrusive Wearable Device,” *Proc. ACM Interact. Mob. Wearable Ubiquitous Technol.*, vol. 1, no. 3, p. 58:1-58:23, Sep. 2017, doi: 10.1145/3132024.
- [39] T. B. Plante *et al.*, “Validation of the Instant Blood Pressure Smartphone App,” *JAMA Intern Med*, vol. 176, no. 5, pp. 700–702, May 2016, doi: 10.1001/jamainternmed.2016.0157.
- [40] M. Kuwabara, K. Harada, Y. Hishiki, and K. Kario, “Validation of two watch-type wearable blood pressure monitors according to the ANSI/AAMI/ISO81060-2:2013 guidelines: Omron HEM-6410T-ZM and HEM-6410T-ZL,” *J. Clin. Hypertens. (Greenwich)*, vol. 21, no. 6, pp. 853–858, Jun. 2019, doi: 10.1111/jch.13499.

- [41] G. B. Moody and R. G. Mark, “A database to support development and evaluation of intelligent intensive care monitoring,” in *Computers in Cardiology 1996*, Sep. 1996, pp. 657–660. doi: 10.1109/CIC.1996.542622.
- [42] A. E. W. Johnson *et al.*, “MIMIC-III, a freely accessible critical care database,” *Scientific Data*, vol. 3, no. 1, Art. no. 1, May 2016, doi: 10.1038/sdata.2016.35.
- [43] Goldberger Ary L. *et al.*, “PhysioBank, PhysioToolkit, and PhysioNet,” *Circulation*, vol. 101, no. 23, pp. e215–e220, Jun. 2000, doi: 10.1161/01.CIR.101.23.e215.
- [44] M. A. Stroud, D. P. James, D. Railton, and P. J. Sowood, “Digital and brachial artery blood pressure measurements during peripheral, cold-induced vasoconstriction,” *Europ. J. Appl. Physiol.*, vol. 68, no. 2, pp. 134–138, Feb. 1994, doi: 10.1007/BF00244026.
- [45] O. Ronneberger, P. Fischer, and T. Brox, “U-Net: Convolutional Networks for Biomedical Image Segmentation,” *arXiv:1505.04597 [cs]*, May 2015, Accessed: Feb. 11, 2020. [Online]. Available: <http://arxiv.org/abs/1505.04597>
- [46] N. Beheshti and L. Johnsson, “Squeeze U-Net: A Memory and Energy Efficient Image Segmentation Network,” in *2020 IEEE/CVF Conference on Computer Vision and Pattern Recognition Workshops (CVPRW)*, Jun. 2020, pp. 1495–1504. doi: 10.1109/CVPRW50498.2020.00190.
- [47] L. Sifre and S. Mallat, “Rigid-Motion Scattering for Texture Classification,” *arXiv:1403.1687 [cs]*, Mar. 2014, Accessed: May 18, 2021. [Online]. Available: <http://arxiv.org/abs/1403.1687>
- [48] F. N. Iandola, S. Han, M. W. Moskewicz, K. Ashraf, W. J. Dally, and K. Keutzer, “SqueezeNet: AlexNet-level accuracy with 50x fewer parameters and <0.5MB model size,” *arXiv:1602.07360 [cs]*, Nov. 2016, Accessed: May 18, 2021. [Online]. Available: <http://arxiv.org/abs/1602.07360>
- [49] L. Saadatifard, A. Mobiny, P. Govyadinov, H. Nguyen, and D. Mayerich, “DVNet: A Memory-Efficient Three-Dimensional CNN for Large-Scale Neurovascular Reconstruction,” *arXiv:2002.01568 [cs, eess, stat]*, Feb. 2020, Accessed: May 18, 2021. [Online]. Available: <http://arxiv.org/abs/2002.01568>
- [50] M. Elgendi, I. Norton, M. Brearley, D. Abbott, and D. Schuurmans, “Systolic Peak Detection in Acceleration Photoplethysmograms Measured from Emergency Responders in Tropical Conditions,” *PLOS ONE*, vol. 8, no. 10, p. e76585, Oct. 2013, doi: 10.1371/journal.pone.0076585.
- [51] M. Poullis, “New formula to calculate mean aortic pressure?,” *The Lancet*, vol. 353, no. 9169, p. 2075, Jun. 1999, doi: 10.1016/S0140-6736(05)77898-3.

- [52] C. Daube, R. A. A. Ince, and J. Gross, “Simple Acoustic Features Can Explain Phoneme-Based Predictions of Cortical Responses to Speech,” *Current Biology*, vol. 29, no. 12, pp. 1924–1937.e9, Jun. 2019, doi: 10.1016/j.cub.2019.04.067.
- [53] A. Botchkarev, “A New Typology Design of Performance Metrics to Measure Errors in Machine Learning Regression Algorithms,” *Interdisciplinary Journal of Information, Knowledge, and Management*, vol. 14, pp. 045–076, Jan. 2019.
- [54] G. Stergiou *et al.*, “A Universal Standard for the Validation of Blood Pressure Measuring Devices: Association for the Advancement of Medical Instrumentation/European Society of Hypertension/International Organization for Standardization (AAMI/ESH/ISO) Collaboration Statement,” *J Hypertens*, vol. 36, no. 3, pp. 472–478, Mar. 2018, doi: 10.1097/HJH.0000000000001634.
- [55] White W B *et al.*, “National standard for measurement of resting and ambulatory blood pressures with automated sphygmomanometers.,” *Hypertension*, vol. 21, no. 4, pp. 504–509, Apr. 1993, doi: 10.1161/01.HYP.21.4.504.
- [56] Eoin O’Brien, W. L. James Petrie, P. L. P. Michael de Swiet, M. B. Douglas G. Altman, and N. A. Andrew Coats, “The British Hypertension Society protocol for the evaluation of blood pressure measuring devices,” *Journal of Hypertension*, vol. 11, no. Suppl 2, pp. S43–S62, 1993.
- [57] M. Simjanoska, M. Gjoreski, M. Gams, and A. Madevska Bogdanova, “Non-Invasive Blood Pressure Estimation from ECG Using Machine Learning Techniques,” *Sensors*, vol. 18, no. 4, p. 1160, Apr. 2018, doi: 10.3390/s18041160.
- [58] J. Esmaelpoor, M. H. Moradi, and A. Kadkhodamohammadi, “A multistage deep neural network model for blood pressure estimation using photoplethysmogram signals,” *Computers in Biology and Medicine*, vol. 120, p. 103719, May 2020, doi: 10.1016/j.combiomed.2020.103719.